



1032716



650037598

Coursework: Final Report**Submission Deadline:** Wed 9th May 2018 12:00**Personal tutor:** Dr Anna Baldycheva**Marker name:** N/A**Word count:** 12000

By submitting coursework you declare that you understand and consent to the University policies regarding plagiarism and mitigation (these can be seen online at www.exeter.ac.uk/plagiarism, and www.exeter.ac.uk/mitigation respectively), and that you have read your school's rules for submission of written coursework, for example rules on maximum and minimum number of words. Indicative/first marks are provisional only.

First marker's comments

Indicative
mark

Second marker's comments

Second mark

Moderator's comments

Agreed mark



Final Report

Numerical Simulations of Plunging Waves Run Up and Overturning in the Surf-Zone.

Stefano Conti

|2018|

3rd Year Individual Project

I certify that all material in this thesis that is not my own work has been identified and that no material has been included for which a degree has previously been conferred on me.

Signed

A handwritten signature in blue ink, appearing to be "Stefano Conti", written over a horizontal dotted line.

Final Report

[ECM3101]

Title: Numerical Simulations of Plunging Waves Run Up
and Overturning in the Surf-Zone.

Date of submission: Tuesday, 08 May 2018

Student Name: Stefano Conti
Programme: Beng Materials Engineering
Student number: 650037598
Candidate number: 053759

Supervisor: Dr. Gavin Tabor

Abstract

To design in-land surfing wave-pools, the wave breaking characteristics used to predict breaking intensity need to be modelled and understood. A Coupled Level Set – Volume of Fluids (CLSVOF) method based on the Navier-Stokes equations has been employed to simulate wave run up and overturning of solitary plunging waves in a 2-dimensional domain. The numerical model used a simple RANS realizable k-epsilon turbulence method for an accurate representation of the turbulent splash-up process. The model was validated against experimental results (Liu, 2000) and a study on the breaking wave characteristics of different plunging breakers was performed. Wave breaking characteristics, such as the surf similarity parameter (SSP), breaker index, breaker height and breaker depth were analysed and evaluated against literature values. The uncertainty and lack of precision of the existing methods was demonstrated - owing to the non-linearity and instability of the wave breaking process – and a novel parameter, the jet thickness ratio, has been presented. This geometrical ratio shows good agreement with literature and, if studied further, has the potential to further the knowledge of breaking wave characteristics for surf amenity. The main limitations of ANSYS – mesh dependency and lack of higher order transient formulations – have been depicted and conclusions to the validity of the project have been drawn.

Acknowledgments

I would like to thank my supervisor Dr. Gavin Tabor for his guidance; this dissertation would have not been possible without his support.

Keywords: CFD, CLSVOF, Plunging Breakers, Breaking Intensity, Surfing

Table of contents

1. Introduction and background.....	1
1.1. Aims and Objectives	1
1.2. Project Breakdown	2
2. Literature review.....	3
2.1. Wave Formation and Characterisation.....	3
2.2. Surfing Design Criteria	5
2.3. Numerical Simulations of Plunging Waves in the Surf-zone	7
3. Methodology and theory.....	9
3.1. Introduction	9
3.2. Measuring Breaking Intensity	9
3.3. Wave Splash Up Process.....	10
3.4. Numerical Model.....	11
3.5. Validation of Numerical Model and Computational Power.....	15
4. Analytical Work	16
4.1. Validation of Code	16
4.2. Breaker Intensity Analysis Set up	20
5. Results and Analysis.....	21
5.1. Qualitative Observations	21
5.2. Breaker Height and Depth.....	22
5.3. Breaking Intensity	23
6. Discussion and conclusions	25
6.1. Discussion	25
6.2. Conclusion.....	26
7. Project management, consideration of sustainability and health and safety	27
References.....	29

1. Introduction and background

In the past 20 years, surfing has grown exponentially, both as a professional sport and as a leisure activity. Surf spots are present on nearly all coastlines around the world, with waves breaking over complex topographies in all shapes and forms. However, world-class surf breaks are limited, and the rising popularity of the sport causes them to be increasingly over-crowded. With the world's best waves being engulfed by the growing crowds and the recent inclusion of surfing in the Olympic 2020 games (Tokyo, 2018), a demand for in-land surfing wave-pools is evident. Wave pool technologies to replicate good surfing conditions have only started to be developed in the past two decades. Recently, companies such as the Kelly Slater Wave Pool Co (Kelly Slater Wave Company, 2018) and Wavegarden (Wavegarden.com, 2018) managed to produce the first full scale world-class in-land surf spots.



Figure 1. Kelly Slater Wave Pool Co Prototype in Lemoore, California (Kelly Slater Wave Company, 2018)

In the present literature, multipurpose reefs for beach protection and surfing have been explored, ranging from evaluations of existing reefs (Johnson, 2009) to numerical methods of planned solutions (Mortensen and Henriquez, 2012). However, wave-pool technologies and their implementation are still scarce. The only thesis present on the topic is a research by De Schipper (2007) on the generation of 'surfable' ship waves in a circular wave pool. Research into breaking wave reaches back 150 years ago. Parameters such as the breaker index (McGowan, 1891) and the Irribarren number (Irribarren, 1949) were the first attempts to quantify the different types of breaker present on coastlines. Breaker height and depth formulas have been further researched (Komar, 1998; Rattanapitikon, 2000; Rattanapitikon, 2003, Goda, 2010; Robertson, 2014), however, the non-linear nature of breaking waves means that the prediction of different types of wave breakers and their intensity are still unclear (Black and Mead, 2001). Clear distinctions between different types of plunging breakers, needed to simulate surfing waves, are missing in literature. As such, this thesis focuses on numerical simulations of 2-D breaking waves on slopes. Wave characterisation of different plunging breakers are depicted, assessing breaker intensity, depth and height. The work on geometrical patterns of plunging breakers as a measure of breaking intensity is brought forward by assessing a new parameter, as advised by Robertson (2014), of jet thickness to wave height at breaking. A CLSVOF approach based on the Navier-Stokes equations is implemented using ANSYS Fluent 18.1 to simulate the breaking waves, and conclusions are drawn to the suitability of this software. The mathematical model is validated against laboratory experiments of wave run up in wave tanks.

1.1. Aims and Objectives

The main aims and objectives of this thesis are to:

1. Investigate the theories behind breaking waves and their interaction with the bottom topography.
2. Create a mathematical model to describe wave run up, overturning and splash up process of shallow water waves in 2D.
3. Evaluate ANSYS Fluent as a tool to simulate ocean waves in the surf zone.
4. Measure and evaluate breaking waves parameters of different waves on a 1/15 slope and compare them with existing theory.

5. Propose a new geometrical parameter, Jet thickness ratio, to assess breaking intensity of plunging breakers.

1.2. Project Breakdown

The project is split in the following sections:

- Chapter 1 introduces the problem and establishes aims and objectives.
- Chapter 2 presents the literature review covering the existing theories of breaking waves and an extensive review of computational methods to simulate overturning waves in the surf-zone.
- Chapter 3 explains the theory and methodology used in this thesis, explaining the general dynamics of the wave breaking process and describing the mathematical model used.
- Chapter 4 shows the validation of the model against experimental results and outlines the analytical work to determine breaking characteristics.
- Chapter 5 shows the results of different simulations, analysing their breaking characteristics and drawing conclusions to the validity of existing theories and the novel jet thickness ratio.
- Chapter 6 discusses the limitations of this project and gives a conclusion summarising the main findings and further recommendations.
- Chapter 7 discusses the project management and risk assessment associated with this dissertation.

2. Literature review

2.1. Wave Formation and Characterisation

When wind strokes the ocean surface, it creates a movement of fluid particles acting as a medium for a wave to travel across. The interaction between the two fluids creates friction that drives waves (Kusterle, 2007). Waves form as capillary waves and slowly, as wind speed increase over two knots (Kinsman, 2002), transition to gravity waves. Gravity waves travel on the water surface level and are held by gravitational forces. They can move across oceans without any forces acting on them if encountering only light head winds (Kinsman, 2002). Once formed, they can travel for days losing very little energy (Kinsman, 2002). The height of gravity waves in open ocean depends on three factors: the force exerted by the wind on the water surface, the duration the wind blows for and the distance over which it blows (Kinsman, 2002).

As ocean gravity waves move out of deep water into the surf-zone area, they begin to interact with the bottom topography. As waves approach the coastline and water depth decreases, the effects of refraction, shoaling and bottom friction start morphing the waves, causing them to undergo certain observational changes. The dispersive nature of wave propagation causes the wavelength to decrease, wave height to increase through shoaling and celerity to decrease (Johnson, 2009). This causes the wave to slow down and the wave face to steepen as a function of water depth decreasing, until the wave finally breaks. There are many factors that account for the shape and size of a wave as it breaks in shallow water. The analysis of water wave breaking has been on-going for almost 150 years, with many authors trying to describe and quantify this non-linear occurrence. Predictions of breaker types (Iribarren) and different techniques to estimate breaker height and depth (Rattantiposky, Goda, Robertson, Komar) are presented in this section.

2.1.1 Breaker Type

Many authors have tried to describe the factors that affect wave breaking in shallow water. Iribarren and Nogales (1949) were the first to define different wave breakers. They characterised them as the ratio between steepness of the seabed slope to the steepness of the wave itself. The Iribarren parameter is described mathematically as:

$$\xi = \frac{\tan \alpha}{\sqrt{H_b/L_o}} \quad (1)$$

Where α is the steepness of the slope, L_o is the deep-water wavelength and H_b is the wave height at breakpoint. Iribarren and Nogales characterized breakers into 3 distinct categories, shown in figure 2. For surfing waves, plunging and spilling breakers are wanted depending on the conditions needed. As the ocean floor steepens, the shape of the breaker transitions from spilling to surging, and the bottom topography plays an increasingly important role. Surging breakers break on extreme slopes, causing them to break very close to shore producing no surf-zone area.

The values of ξ used to describe the breaker types are:

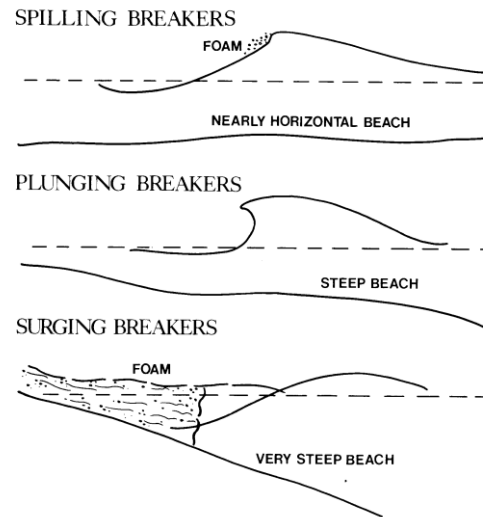


Figure 2. Different types of breakers. (Black and Mead, 2001)

Table 1. Iribarren parameter values

Breaker type	Value ξ
Spilling	$\xi < 0.4$
Plunging	$0.4 < \xi < 2.0$
Surging/Collapsing	$\xi > 2.0$

The Iribarren parameter as derived by Iribarren and Nogales (1949) assumes a wave propagating from deep water with wavelength L_0 , breaking in shallow water. However, as outlined by De Schipper (2007), this was an inconvenient way to compare breaker types as the waves are not generated in deep water. As such, (1) was reformulated as:

$$\xi = \frac{\tan \alpha}{\sqrt{2\pi \frac{H_b d_b}{L_b^2}}} \quad (2)$$

Where H_b , d_b and L_b are wave height, water depth and wavelength at breakpoint, respectively. Equation 2 was derived using linear wave theory and is available in De Schippers (2007) work at pg.20.

2.1.2 Breaker Depth and Height

When waves enter the shallow waters, their breaking is no longer limited by the wavelength. Water depth and slope of the seabed also start playing an important role. Breaker depth is defined as the water depth at which a wave begins to break, this is the point where the wave reaches its limiting steepness and topples over (Johnson, 2009).

The wave height and water depth at breaking can be derived using empirical formulas and linear wave theories. In 1981, Mc Gowan (1891) in his work on solitary waves described the two parameters to be linked, for horizontal slopes, by the relationship:

$$\frac{H_b}{d_b} = 0.78 \quad (3)$$

Equation 3 was very simplistic and has been developed throughout the years. However, the ratio H_b/d_b , also known as the breaker index, has been used ever since as a measure of breaking intensity. Miche (1944) showed how the breaking wave height was determined by the waves wavelength at which it travels. Miche (1944) based his work on linear wave theory and considered the horizontal orbital velocity of the water particles at the crest of a wave to be equal to the wave celerity for breaking to occur. With further development in the field and more experimental data available to researchers, recent breaker indices have been proven to be more accurate. Komar (1998) noted how most breaker indices relied on both breaker depth and height, making them difficult to be extracted. The study suggested:

$$H_b = 0.39 g^{0.2} (T_w H_o^2)^{0.4} \quad (4)$$

$$d_b = H_b \left\{ 1.2 \left[\frac{m}{(H_b/L_o)} \right] \right\}^{-0.17} \quad (5)$$

Where T_w is the wave period, m is the slope of the seabed and H_o is the deep-water wave height.

Rattanapitikon and Shibayama (2000) noted the lack of slope dependence in Komar's (1998) equations and came up with a revised formula for breaker depth and height based on Goda's (1970) work. The study compares 24 experimental results to develop an exponential relationship of the form:

$$H_b = 0.17L_o \left(1 - e^{\left[\frac{\pi d_b}{L_o} (16.21m^2 - 7.07m - 1.55) \right]} \right) \quad (6)$$

In 2003, Rattanapitikon and Shibayama (2003) analysed another 26 sources and noted how the best fit to the data was given by the power law between the breaker height and deep-water wave length for both breaker height and depth. They proposed:

$$H_b = (-1.4m^2 + 0.57m + 0.23)L_b \left(\frac{H_o}{L_o} \right)^{0.35} \quad (7)$$

$$d_b = (3.86m^2 - 1.98m + 0.88)H_o \left(\frac{H_o}{L_o} \right)^{-0.16} \quad (8)$$

These equations hold true for cases with $m < 0.38$ and $\frac{H_o}{L_o} < 0.1$ and should not be used outside the values.

Goda (2010) revised his previous experimental work in spite of Rattanapitikon and Shibayama's (2000) findings, and proposed:

$$H_b = 0.17L_o \left(1 - e^{\left[\frac{-1.5\pi d_b}{L_o} (1 + 11m^{\frac{4}{3}}) \right]} \right) \quad (9)$$

In 2014, Robertson (2014) presented a novel, low cost method to extract wave breaking properties from irregular waves in the surf zone, using optical and in-situ measurement systems. From his results, he proposed a breaker height formula based on an exponential function:

$$H_b = 0.17L_o \left(1 - e^{\left[\frac{\pi d_b}{L_o} (1.978m - 1.792) \right]} \right) \quad (10)$$

Robertson (2014) noted how equation 10 was based on the measured data, which does not cover all possible breaking conditions, and should only be applied within the limits of the presented data.

2.2. Surfing Design Criteria

The objective of a surfer is to ride the unbroken face of a wave as it progresses across different sections. A wave section is a part of a wave that peals at constant speed and angle. Ocean waves comprise of different sections dependant on the breaker intensity, peel angle, slope of the seabed and effects of refraction. The quality of these sections depends on the shape of the wave, the speed at which it breaks and the intensity of the ride. Both plunging and spilling breakers are required for favourable surfing conditions. The former exhibits a hollow powerful wave where barrel riding (riding between the plunging jet and the face of a breaking wave) is possible. The latter gives a slower, open face wave, where a variety of manoeuvres can be performed. To simulate ocean waves indoors, an understanding of the breaking intensity needed to give different plunging breakers is needed. The Iribarren number, also known as the Surf Similarity Parameter (SSP, eqn. 2), is very simplistic, and has been found to inaccurately describe breaking events (Mead, 2001). With the advent of more

data, authors have started to describe plunging breakers in more depth, using curve fitting to find vortex ratios and vortex angles (Longuett-Higgins 1982; Mead 2001; Johnson 2009; Robertson 2014) to measure the intensity of a plunging breaker.

2.2.1. Peel Angle

One of the most important parameters in the design of an indoor wave is the peel angle. It is the critical term used to describe the speed that a surfer needs to travel to successfully traverse the face of a wave (Mead, 2003). Good surfing waves break in ‘peeling’ manner, and, depending on the peel angle can change between a challenging and a beginner-friendly wave. Figure 3 shows a typical surfing wave, with the relationship between wave celerity C , peel angle α and surfer velocity to ride the section of the wave (Johnson 2009). Due to the vector relationship displayed in figure 3, different peel angles can be used (0-90°) modifying the wave direction and topography of the seabed, to give faster or slower sections. The wider the angle, the faster and more challenging the wave will be. Mead (2003) and Johnson (2009) give comprehensive descriptions of surfing hydrodynamics for designing artificial reefs. These papers outline the wave characteristics extensively.



Figure 3. Peel angle parameters (Johnson, 2009)

2.2.2. Vortex Ratio and Breaking Intensity

In order to quantify the intensity of a plunging breaker, Longuett-Higgins (1982) proposed a parametric description of incompressible, irrotational flow to describe the vortex created by a plunging breaker in side view. He proposed the following equations to describe the shape of the breaker mathematically:

$$\frac{x}{t^4} = 3\mu^2 - 13 \quad (11)$$

$$\frac{y}{t^4} = -\mu^3 + 2\mu \quad (12)$$

Where x and y are spatial co-ordinates measured from an axis of symmetry, t is time and μ is a variable used to separate real and imaginary parts. Using equations 11 and 12, Mead and Black (2001) came up with a method for predicting and describing breaking intensity of plunging surfing waves. They measured images of high quality surfing breaks and used the curve fitting method to measure the wave height and vortex ratios. The parameters were measured according to figure 4 and the vortex ratio was calculated as:

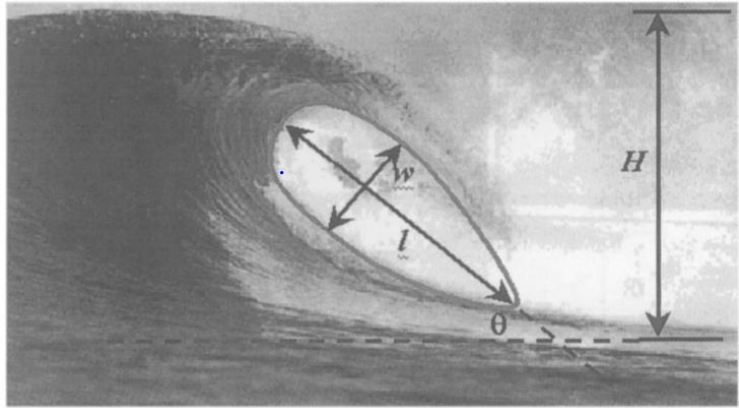







Figure 4. Vortex Ratio Calculations (Black and Mead, 2001)

$$r_v = \frac{l_v}{w_v} \quad (13)$$

Where l_v and w_v are the vortex length and width, respectively, and r_v is the vortex ratio. After analyzing different surf breaks, Black and Mead found a good correlation between vortex ratio, wave heights and seabed slopes, and proposed the following relationship:

Table 2. Classification of breaking intensity with vortex ratio (Black and Mead, 2001)

Intensity	Extreme	Very High	High	Medium/High	Medium
Vortex Ratio, r_v	1.6 - 1.9	1.91 - 2.2	2.21 - 2.5	2.51 - 2.8	2.81 - 3.1
Wave Shape					

They also noted that the vortex angle, shown in figure 4, did not affect the intensity of the break.

Johnson (2009) and Robertson (2014) both conducted experimental research on vortex ratios and angles concluding that the only consistent trend between vortex parameters and wave characteristics was a lack of significant dependence, suggesting that vortex ratio and angle are insufficient to predict the breaking intensity of waves and should not be investigated further. However, Robertson (2014) advised that further work on geometrical parameters of plunging waves could be done to give insight into the wave vortex intensity theory such as the jet thickness over the breaker height ratio, which has been considered in this study.

2.3. Numerical Simulations of Plunging Waves in the Surf-zone

Over the last few decades, advances in experimental and theoretical work in the surf-zone hydrodynamics led to the creation of various mathematical models to describe wave creation, shoaling and overturning in the surf zone. Due to the high-complexity and non-linearity of the problem, these models had mixed results, and only recently, three-dimensional overturning waves over complex topography have been investigated. Additionally, the post-breaking process, with air entrainment and jet splash up cycles, further complicates the problem.

There are essentially two types of mathematical models for modelling overturning waves (Xie, 2015). The first model is the fully nonlinear potential flow based on Laplace's equation with inviscid and irrotational assumptions. This model is quite simplistic and only simulates breaking waves up to overturning. Even though the potential flow models are very computationally efficient, they do not have the required precision and cannot provide any information after wave breaking in turbulent flows (Xie, 2015).

The second mathematical model for modelling breaking waves is based on the Navier-Stokes equations with free surface calculations. To capture the air-water interface, various methods have been employed. Among these, the most common are the Volume of Fluid (VOF) (Cheng et al, 1999; Hieu et al, 2004; Xie, 2015), Level Set (Hendrickson, 2005) and Coupled Level Set + Volume of fluids (Liu et al, 2016; Wang et al, 2009; Keshavarzi et al, 2012) methods. Among these methods, there are one phase flow models, in which air pressure is taken as constant and disregarded, and only water is modelled. These models describe well the dynamic characteristics of the wave up to overturning, however, they are simplistic and fail to describe the air entrainment inside a plunging wave breaking. In order to take into account the air entrainment in the overturning and splash up process, 2D and 3D two phase flow models have been developed.

In the 2D cases, various two-phase flow models have been employed to describe the phenomenon. Chen et al (1999), Hieu et al (2004) and Wang et al (2009) used a two-phase flow VOF model, with a simple RANS k-epsilon turbulence model to describe the turbulent flow in the post-breaking. The main advantages of the VOF model is the capturing of the general dynamic features of a breaking wave with a relatively reduced computational effort. However, the details of the flow near the crest of the wave are hardly distinguishable with this method. As such, Liu (2016) proposed a coupled level set VOF method (CLSVOF) to account for the complex geometry as well as the surface tension present. The coupling takes the advantage of the level set method in the accurate representation of the dynamic processes accompanied by the complex evolution of the surface with the restricted computational effort of VOF. The simple k-epsilon turbulence model in 2D can describe the wave formation and overturning well, however it can only be implemented on a sloped beach, and wave sections and real seabed bathymetries cannot be simulated. However, a simple 2D CLSVOF method can give good insight on wave breaking and the geometrical patterns that describe plunging breakers.

To fully describe an ocean wave, three-dimensional problems need to be modelled with a suitable turbulence model. Various attempts have been made, Lubin et al (2006) investigated a two-phase flow of deep-water periodic breaking waves over constant water depth, Mutsuda (2000) described breaking waves over a double reef and Lakehal & Liovic (2011) studied the turbulence structure in breaking waves over a plane slope. One of the most challenging modelling aspects is the correct representation of the turbulent flow in the post-breaking section of the wave. The most widely used turbulence model is the Large Eddy Simulation (LES). In this approach, only large-scale eddies are computed directly and a low-pass spatial filter is applied to the instantaneous conservation equations to formulate the 3D unsteady governing equations for large-scale motions. Lubin et al (2006), Mortensen and Henriquez (2012) and Xie (2015) all use LES for the correct representation of the turbulent flow phase. Xie's (2015) develops a two-phase flow model to study three-dimensional breaking waves over complex topography. Xie employs a LES approach, based on the filtered Navier Stokes Equation with a Smagorinsky sub-grid model used for the unresolved scale of turbulence. The governing equations are discretized using the finite volume method, with a PISO algorithm being employed for the pressure-velocity coupling. This study shows some great results of wave breaking on plane slopes and complex topographies, accurately showing the post-breaking process. This approach is considered the best up to date, however, its main drawbacks are the computational expense associated with the LES turbulence model and the higher order solvers required for this method to work. As shown later, the heavy LES model, coupled with a very fine grid for interface capturing, made this turbulence model inadequate with the resources available.

3. Methodology and theory

3.1. Introduction

To understand the dynamics of wave formation and breaking, a mathematical background of the nature of the problem and the numerical method used to solve it are needed. Due to the incredible amount of computational expense needed to create 3D simulations (as discussed in chapter 7), this study focuses on wave breaking on a slope in a 2D domain. Not being able to simulate in 3D means that wave sections and wave-pool reefs cannot be simulated, shifting the focus of this paper to a description of the wave characteristics and breaking intensity. After the code has been validated, different waves are simulated on a 1/15 slope and are characterised. A new method to quantify breaking intensity is considered, and the general breaking characteristics of plunging breakers are introduced. Furthermore, the numerical model used and the mathematical theories describing wave formation in shallow water are described.

3.2. Measuring Breaking Intensity

To measure the breaking characteristics of a wave, the key components must be defined. Considering the 2-D domain shown in figure 5, the wave height and water depth of the breaker, H_b and d_b , were calculated when the wave face became vertical (Sayce, 1998). This marked the point where the particle velocity in the water was equal to the wave celerity (Johnson, 2009), and signaled where the wave started to topple over. Both these measurements were taken with regards to the still water level (SWL), the sea level when no waves are present.

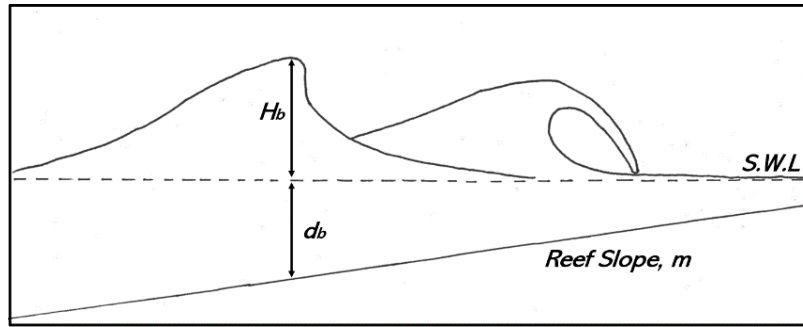


Figure 5. Description of the general problem of wave breaking

All measurements were taken using ANSYS CFD-Post. Once the values for H_b and d_b were extracted, the breaker index:

$$\gamma = \frac{H_b}{d_b} \quad (14)$$

was calculated. Using the time period output from ANSYS, the deep water and breaking wavelength, L_o and L_b , were calculated using linear theory as (De Schipper, 2007):

$$L_o = C_{deep} T = \frac{gT^2}{2\pi} \quad (15)$$

$$L_b = C_{shallow} T = \sqrt{gd_b} T \quad (16)$$

Knowing the wavelength, wave height, depth at breaking and slope of the beach, the surf similarity parameter (eqn. 1 and 2) and literature values of wave height and depth (eqn. 4-10) have been compared to the simulation.

Theoretically, as the slope of the beach increases, the breaker index, and thus breaking intensity, increases (Black and Mead, 2001). However, the non-linearity and irregularity of breaking waves renders the transitions

points between different types of breakers unclear, as the SSP has been proven to often misjudge the type of breaker, especially in the spilling/plunging transitional point. (Black and Mead, 2001; Johnson, 2009).

A distinction between intensity of different plunging breakers had been attempted by Black and Mead, that correlated vortex ratios (eqn. 13) to the intensity of different plunging breakers. The study was later discarded by different authors for the lack of correlation and statistical dependence. (Johnson, 2009, Robertson, 2014).

To predict waves in a wave-pool, a quantitative relationship to distinguish between the intensity of plunging breakers is needed. As advised by Robertson (2014), this study proposed to investigate the ratio of thickness of jet, J_t , and wave height at break point, H_b , as follows:

$$\rho = \frac{J_t}{H_b} \quad (17)$$

where ρ is the Jet thickness ratio.

As shown in figure 6, the jet thickness was measured from the thickest point of the vortex of the plunging breaker up to the crest of the wave. The measurement was taken when the lip of the wave first impacted the surface of the water.

As stated by Li (2000), if the impingement point of a plunging jet is located on the free surface ahead of the jet, a splash up including a reflected jet is formed which further increases the turbulence and energy dissipation associated with wave breaking. Therefore, as jet thickness increases, the mass of water which is displaced in the wave breaking process increases. As more mass is projected outside the wave, the energy dissipation and thus the breaking intensity of the wave must increase. Due to the jet thickness increasing as plunging breakers transition into collapsing breakers, eqn. 17 should increase, showing that relative to the wave height, a thicker jet gives a more intense breaker.

Analysed against the breaker index and the surf similarity parameter, the jet thickness ratio should show a positive correlation owing to the assumption stated above.

3.3. Wave Splash Up Process

After a plunging wave breaks, it undergoes a splash-up process which, depending on water depth, has certain observational characteristics independent of wave height. Figure 7 shows a sketch (Liu, 2000) of the vortices generated by a plunging breaking wave. A total of two impingements and two splash-ups of air-water mixture can be observed during the process. As the waves breaks, the overturning jet impinges the water surface to form the first clockwise roller and generates the first bubble cloud (Lim et al, 2014). This is where a surfer would position himself to perform a ‘barrel’. Barreling is the most sought out manoeuvre in surfing, and the main reason, together with speed and intensity, that a plunging breaker is needed. Directly after the jet hits the water surface with large momentum, the water surface breaks and is pushed forward, forming the first foamy splash-up and generating the second clockwise rolling bubble cloud (Lim et al, 2014). If the jet penetrates deep enough, a counter-clockwise vortex is formed between the two bubble clouds (Liu, 2000). If the wave

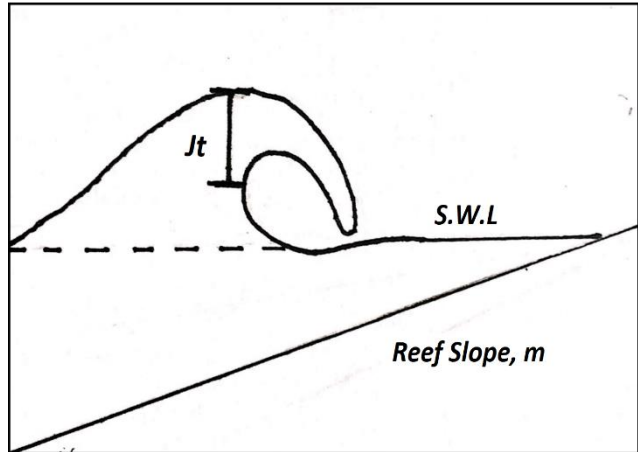


Figure 6. Geometry of the plunging breaker and specification of the jet thickness measurements.

breaks too close to the shore of the beach, the jet generated impinges the dry slope and a reflected jet is not produced. In this case, the wave collapses when it breaks (Liu, 2000).

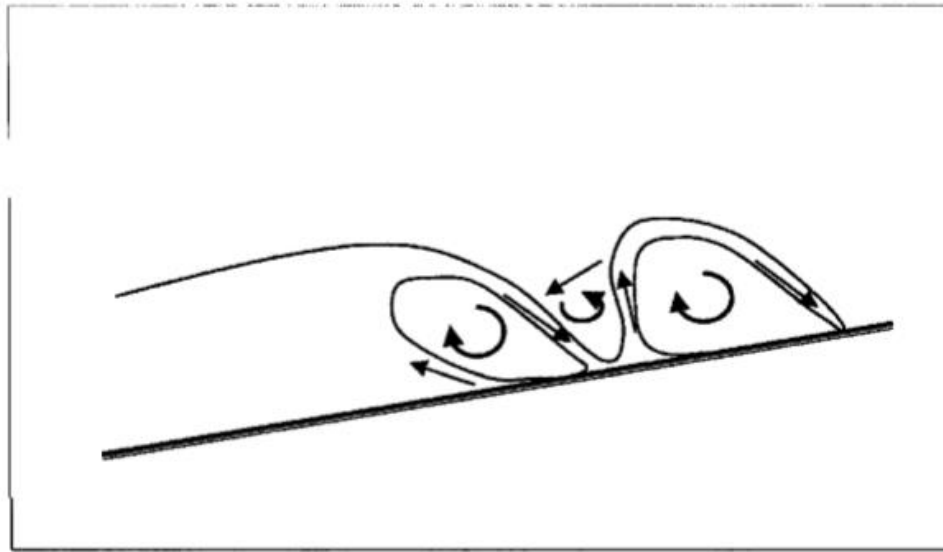


Figure 7. Illustration sketch of the vortices generated by the plunging breaker. (Liu, 2000)

3.4. Numerical Model

Based on the literature review, a two-phase flow model with a CLSVOF method based on the Navier-Stokes governing equations was employed. The governing equations were discretized with a Finite Volume Method (FVM) and the PISO algorithm was adopted for pressure-velocity coupling. The high resolution geo-reconstruct interface capturing scheme was used to give the best possible visual representation of the breaking waves. The simulations were ran using an explicit time-stepping method. The advantages of using a LES turbulence model have been outlined in section 2.4, however, this method posed some major problems that led to it being discarded as the final solution. Firstly, due to the three-dimensional nature of representing turbulence in LES, using this method in 2D is not advised and it does not give an option to do so on ANSYS. Also, the LES model requires an incredible amount of computational power, as it needs a great precision in meshing and higher order schemes to run properly. The higher order schemes posed the greatest limitations, as Fluent forces to use a first order implicit transient formulation which was not precise enough to resolve the large eddies scales and smaller sub-grid turbulences in the LES approach. For simplicity, a realizable k-epsilon turbulence model was chosen as it represented, especially in 2-D, a low computational expense method to correctly interpret the wave breaking and splash-up process. The spatial discretization of momentum, turbulent kinetic energy, dissipation rate and level-set function were all set to second order to maximise the precision of the model.

To simulate ocean waves, ANSYS offers an ‘Open Channel Wave Boundary Conditions’ package that enables users to create waves according to different shallow and deep-water theories. In the shallow-water regime, two mathematical theories were available: Solitary and Cnoidal. Based on Fenton’s (1998) solution, Cnoidal/Solitary wave theories are expressed using complex Jacobian and elliptic functions and are briefly described below.

3.4.1 Governing Equations and the Coupled Level Set – Volume of Fluid Method

The continuity and momentum equations that govern the motion of Newtonians fluids based on the one-fluid formulation are given by (Keshavarzi et al, 2012):

$$\frac{\partial \rho}{\partial t} + \nabla \cdot (\rho U) = 0 \quad (18)$$

$$\frac{\partial(\rho U)}{\partial t} + \nabla \cdot (\rho U \otimes U) = -\nabla p' + \nabla \cdot (\mu \nabla U) + (\rho - \rho_0)g + F_\sigma \quad (19)$$

Where U and ρ are the mixture velocity and density, respectively, p is the modified pressure based on $p' = p + \frac{2}{3}\mu \cdot U - \rho_0 g x$ where ρ_0 is the reference density, g and x are the gravity and coordinate vectors, respectively, μ is the mixture dynamic viscosity and F_σ is the volumetric surface tension force vector. The level set and volume of fluids method decide the momentum and continuity equation through the establishment of the dynamic viscosity and density of the mixture.

The level set method is a popular interface-tracking method for computing two-phase flow with topologically complex interfaces (ANSYS, 2012). Similarly to a VOF method, the interface is captured and tracked by the level-set function, defined as a distance from the interface. Due to the level set function being smooth and continuous, its spatial gradients can be accurately calculated (Osher, 1998). Therefore, the level-set method provides an accurate estimate of interface curvature and surface tension caused by the curvature (ANSYS, 2012). The main drawback of this method is the deficiency in preserving volume conservation (Olsson, 2007). In the LS method, a level function f is defined. The evolution of the function is given by (Keshavarzi et al, 2012):

$$\frac{\partial \phi}{\partial t} + U \nabla \cdot (\phi) = 0 \quad (20)$$

This function is zero at the interface, positive on one side and negative on the other side. The phase properties can be interpolated across the surface as (Keshavarzi et al, 2012):

$$\rho = ((1 - H(\phi))\rho_{gas} + H(\phi)\rho_{liquid}) \quad (21)$$

$$\mu = ((1 - H(\phi))\mu_{gas} + H(\phi)\mu_{liquid}) \quad (22)$$

Where ρ and μ are the density and dynamic viscosity, respectively. The Heaviside function $H(\phi)$ is given in ANSYS (2012) as:

$$H(\phi) = \begin{cases} 0 & |\phi| > a \text{ (gas phase)} \\ 1 & |\phi| > a \text{ (liquid phase)} \\ \frac{1}{2} \left[1 + \frac{\phi}{a} + \frac{1}{\pi} \sin\left(\frac{\pi\phi}{a}\right) \right] & |\phi| \leq a \end{cases} \quad (23)$$

Where a is the distance from the interface.

The VOF method, on the other hand, is naturally volume-conserved, as it computes and tracks the interface using a volume fraction function F that indicates the presence of either gas or liquid phase within each cell. F specifies the fraction of the volume of each cell by giving it a value of $F = 1$ if the cells are filled with the liquid phase and $F = 0$ for cells containing only the gaseous phase. A value between zero and one ($0 < F < 1$) means that the cell contains both phases, indicating an interface between the two fluids passing through these cells. The scalar advection equation for volume fraction F is solved according to (Keshavarzi et al, 2012):

$$\frac{\partial F}{\partial t} + \nabla \cdot (UF) = F \nabla \cdot (U) \quad (24)$$

The mixture density and viscosity can then be described based on the linear dependence on the distribution of F as:

$$\rho = ((1 - F)\rho_{gas} + F\rho_{liquid}) \quad (25)$$

$$\mu = ((1 - F)\mu_{gas} + F\mu_{liquid}) \quad (26)$$

The main advantages of VOF include the mass conservation, computational efficiency and ease of implementation (Xie, 2015). However, the LS method is a more accurate methodology in capturing the interface, due to the discontinuity of the VOF function (the volume fraction of the phase) across the interface.

By coupling the LS and VOF methods, the accuracy of the smooth LS function can be coupled with the computationally efficient volume conservation properties of the VOF method, to overcome the deficiencies of the two approaches. To couple the LS and VOF methods the distribution of the volume fraction F is reconstructed from the LS function ϕ , providing a sharp determination of the interface. Both F and ϕ are then advected through their respective transport equations. Then the LS function, ϕ , is reconstructed based on the F function and reinitialized. The pressure and velocity coupling are then calculated based on the new LS function, ϕ . The reinitialization of the LS function in ANSYS (2012) is done via the geometrical method with a piecewise linear interface construction (PLIC). The geo-reconstruct explicit volume fraction spatial discretization scheme is used as its interpolation scheme gives the most accurate and sharp interface resolution. For a better understanding of the model, Keshavarzi et al (2012) offer a full evaluation of the VOF, LS and CLSVOF models in their study on interface capturing of rising bubbles.

3.4.2 Turbulence Model, Pressure-Velocity Coupling and Spatial Discretization

To simulate the complex two-phase flow, an adequate turbulence model was needed for the correct representation of the breaking and post-breaking splash up processes. The LES model offered the most precise method, but due to the unavailability of the method on ANSYS for 2-D domains and the heavy computational expense, a realizable k-epsilon model was chosen.

The realizable k-epsilon model is a relatively recent development and differs from the standard k-epsilon method in two important ways (ANSYS, 2014):

- The realizable k-epsilon model contains a new formulation for the turbulent viscosity.
- A new transport equation for the dissipation rate, epsilon, has been derived from an exact equation for the transport of the mean-square vorticity fluctuation.

The main advantages of using the realizable k-epsilon model are: (i) it predicts more accurately the spreading rate of both planar and round jets; and (ii) it provides superior performance for flows involving rotation, separation and recirculation (ANSYS, 2014). Moreover, the model shows substantial improvements from its standard counterpart where the flow features include strong streamline curvature and vortices, as in the case for this study.

The pressure velocity coupling was obtained by using the PISO algorithm. PISO is used to calculate the corrected pressure twice and after solving the pressure correction equations, the updated pressure and velocity are added by the pressure and velocity correction terms. (Xie, 2015) A better look at the PISO algorithm is given in Xie (2010).

To discretize the governing equations, the FVM was used. The method offers a strong coupling between pressure and velocity and works by dividing the domain into a number of control volumes, such that each control volume surrounds a grid point. The differential equation is integrated over each control volume to derive the algebraic equation for each grid point. (Xie, 2015) The FVM best suits the modelling of free surface flows, as it can deal with complex geometries and has good mass conservation properties (Xie, 2015; Ferziger and Peric, 2002). Xie (2015) gives a full mathematical description of the Finite Volume Method.

3.4.3 Solitary and Cnoidal Wave Theories

To simulate surface gravity waves Fluent gives the option to impose ‘Open Channel Wave Boundary Conditions’ at the inlet. It creates waves by imposing velocity and surface elevation solutions of different wave theories. In the limit of shallow water, Fluent enables users to use two water waves theories: Solitary and Cnoidal. To understand the dynamics and limitations behind the simulation of the wave breaking process, a description of these theories is needed.

Cnoidal wave theory was first derived by Korteweg and de Vries (1895) in their work on the propagation of waves over a flat bed, using a similar approximation to Boussinesq (1871). They obtained periodic solution which they termed ‘cnoidal’ because of the surface elevation being proportional to the square of the Jacobian elliptic function $cn()$. The cnoidal solution shows long flat troughs and narrow crests similar to those observed in real shallow water waves (Fenton, 1998). In the limit of an infinite wavelength, the solution describes a solitary wave.

Due to the complex nature of the Jacobian elliptic functions, Cnoidal theory was not developed for several years. Only recently, with Fenton’s (1998) work on Cnoidal theory of water waves, a 5th order solution has been reached that renders the theory applicable in a range of fields. Fenton (1998) managed to generate a high order solution that was described in terms of rational numbers instead of floating point numbers, simplifying the use to practitioners.

A full mathematical description of Fenton’s (1998) theory is not given in this thesis, as it would take an excessive amount of space and would be futile to the final scope of the thesis. Instead, a distinction between Solitary and Cnoidal theories is shown below. For a full recount of the theory, see: Fenton (1998).

The solution for surface elevation, horizontal and vertical fluid velocities and wavelength are all presented in Fenton (1998, pg.12) as a function of wave height relative to trough depth, solved with respect to the Jacobian elliptic function, $cn(m|z)$, where m and z are the modulus and argument of the function, respectively. It was found, originally by Iwagaki (1968) and then Fenton (1998), that for waves which are not low or short, the values of the parameter m used in practice are very close to unity (Fenton, 1998). Solitary wave theory differs from Cnoidal theory by assuming that the waves have infinite wave length, and as such m is always equal to 1. This makes Solitary wave theory less computationally expensive, and as shown below, more desirable for this thesis, as CPU time was the main limitation encountered.

3.4.4 Meshing

One of the most important aspects for the correct simulation of the problem was a correct meshing practice. Due to the relatively simple geometry used and the great computational expense incurred in simulating, an efficient, yet precise, mesh was needed. To ensure stability in the complex free surface profile tracking of breaking waves, quadrilateral elements have been considered as the best option. Compared to triangular elements, ‘quads’ all have linear terms. As such, the aspect ratio of these elements can be controlled close to one and skewness will be less pronounced than in triangular elements. This ensures displacements to be

interpolated to higher degrees, resulting in a more accurate representation of the flow whilst being computationally efficient.

3.5. Validation of Numerical Model and Computational Power

To validate the mathematical model, Li's (2000) experimental work of wave run up and breaking in a water tank was simulated. Li (2000) performed a series of experiments to obtain wave amplitude time-histories, water particle velocities and wave free surface profiles and compared them with analytical and numerical models. One experiment from Li (2000), wave breaking on a 1/15 slope, was simulated to validate the code. Two cases were simulated with deep water wave heights of $H_o = 0.137$ m and $H_o = 0.122$ m. The former was considered for wave overturning up to when the jet touches the still water level, whilst the latter was used to compare the splash up process. For wave overturning, Li (2000) produced a set of graphs showing the detailed breaking of the 0.137m wave at different time steps, from when the wave crest becomes vertical up to when the plunging lip hits the still water level. These were digitized, using a software called DigitizeIt, that enables you to set a co-ordinate axis on an image and trace points on it. After being graphed, the free surface profiles of the plunging breaker were compared graphically with the simulated case. For the splash-up process, qualitative images of the 0.122m wave were compared with the simulated case and the general dynamics of the splash-up process as describes in section 3.3 was analyzed.

All the simulations were run on a High Computational Power (HPC) server machine. The HPC has 2*14 core Xeon processors and 256 GB RAM and represent a significant computational resource. The average computational time required for the simulations was 5 hours running on 7 processors.

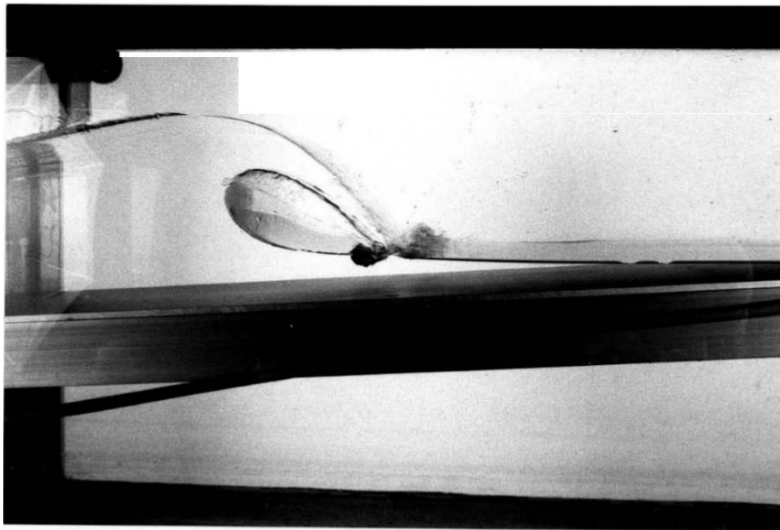


Figure 8. Photograph of typical plunging breaker from Liu's (2000) experiment. (Liu, 2000)

4. Analytical Work

4.1. Validation of Code

4.1.1. Simulation set up

The case set up, including a section on the importance of mesh refinement for the correct simulation of plunging breakers, is given below.

4.1.1.1. Geometry

The 2-D geometry used in the simulation was based on Li's (2000) Caltech west tank (CWT) used for the simulation of breaking solitary waves. The geometry was drawn using the Design Modeler present in ANSYS. The domain was 4.572 m long, 0.5334m tall at the inlet and 0.2286m tall at the outlet. The reef seaward slope was of $m = 1/15$, and the still water level was taken as S.W.L = 0.3048 m from the origin. Figure 9 shows the geometry when initialized at $t = 0$. The contours are colored by water volume fraction. From here on water is shown in red and air is shown in blue.

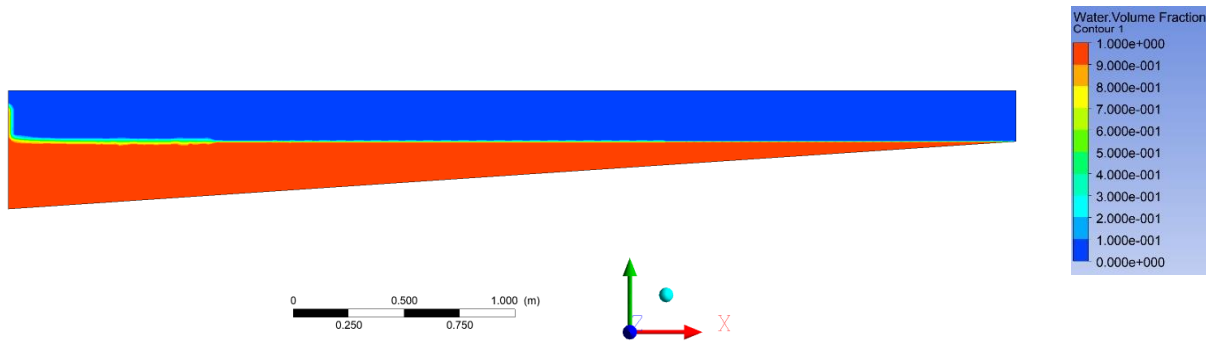


Figure 9. The geometry of the 2D reef considered for wave breaking after initialization.

4.1.1.2. Meshing and Mesh Refinement

The meshing technique used for the geometry was crucial for the functioning of the simulation. As observed in figure 9 and 10, the final mesh had three distinct meshing zones. Zones 1,2 and 3 have cell dimensions of 0.015m, 0.00547m and 0.002735m, respectively. The mesh was finest in the wave breaking area, as great detail was needed to correctly

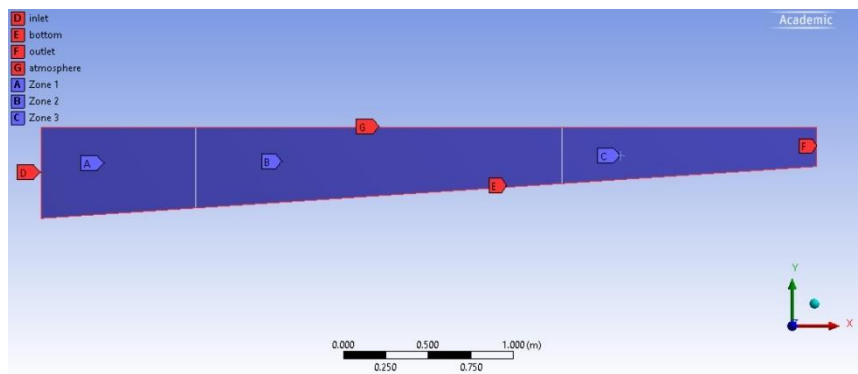


Figure 10. Geometry with meshing zones and boundary conditions.

represent the vortex creation and splash-up process of the plunging breakers. To ensure stability of the wave, the geometry was meshed with a quadrilateral dominant method. The meshing was so case-dependent that by slightly changing the values of zone 2 or 3, the model enormously underestimated the wave height, often causing the wave not to break at all. The mesh-dependency and long computational times were the main reason that wave breaking was only

considered on this geometry as the author failed to find the right mesh for other slopes in the time given. Zone 1 served to stabilize the shape and velocity of the wave at the inlet. To show the importance of the coarser zone 1, a second mesh was tested for validation with zones 1 and 2 merged and given the latter's dimension. The cell number of the final mesh was 84450 cells.

4.1.1.3. *Boundary and Initial Conditions*

Shown in figure 10 are the four boundary conditions. The inlet was set as a velocity inlet, and the 'open channel wave boundary' setting was used to create the wave. Solitary wave theory was chosen over Cnoidal as the former saves significant computational time. The deep-water wave height was set in the velocity inlet, and for the validation it was set at a value of $H_0 = 0.137\text{m}$ for overturning and $H_0 = 0.122\text{ m}$ for the splash-up process. The outlet was considered a pressure outlet, the atmosphere was considered as a symmetry and the bottom slope was set to be a wall. The time step was set to 0.00025 s for a total of 12000 timestep and 3 seconds of simulation. Each timestep was repeated for 40 iterations. A solution convergence graph has not been included due to the space restriction. However, it demonstrated the continuity, momentum, turbulence and transient residuals declining rapidly through the iterations of each time-step. All the residuals reached the cut-off point of 1×10^{-3} for each timestep. The greatest instability was recorded at the wave inlet and decreased as the wave progressed to the breaking area.

4.1.2. *Validation*

4.1.2.1. *Run up and Breaking*

Figures 11 and 12 show the breaking and vortex creation for two cases. The former has a double-zone mesh, missing the coarser zone 1, whilst figure 12 uses the mesh described in figure 10. In figures 11 and 12 (a), the wave crest is becoming vertical, at this point wave celerity approaches water particle velocity, and the wave is considered to be breaking (Johnson, 2009). After this happens, the water particle velocity becomes greater than wave celerity, causing the plunging jet to detach from the wave and catapult itself forwards, leading to figure 11 and 12 (b). To validify the simulations, graph 1 and 2 compare the free surface profiles of the two-simulated cases with Liu's (2000) experiment. For clarity, the x and y axis are expressed as a dimensionless number as $x/\text{S.W.L}$ and $y/\text{S.W.L}$.

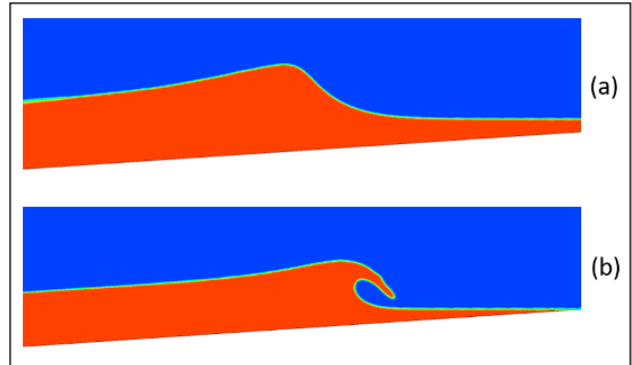


Figure 11. *Qualitative snapshots of breaking wave and vortex creation with double zone mesh.*

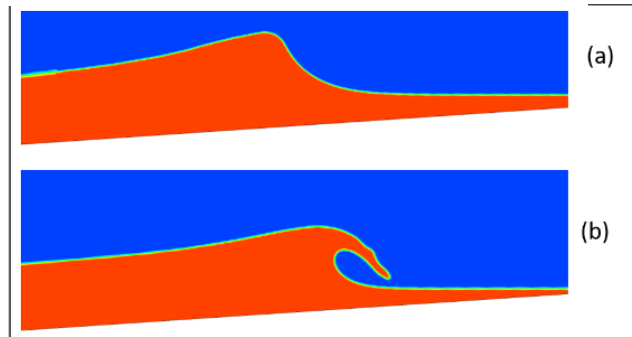
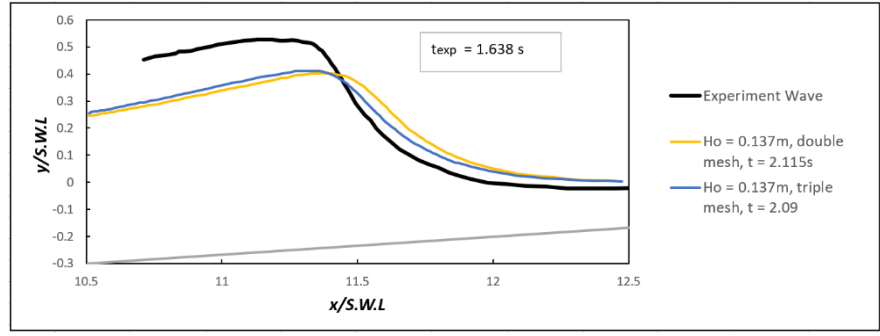
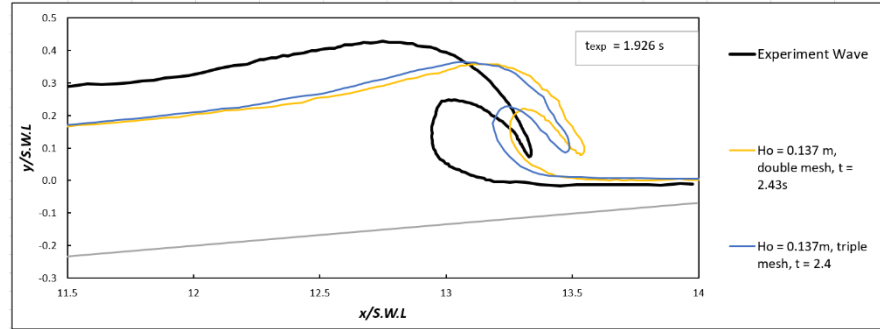


Figure 12. *Qualitative snapshot of breaking wave and vortex creation with triple zone mesh.*

Clearly, the simulation underestimated the wave height at breaking, resulting in a wave that braked slightly ahead of the experiment. The coarser zone increased the stability at wave inlet, causing the wave to be translated quicker and to achieve a higher breaking height. This can be observed in graphs 1 and 2, where the triple mesh wave (shown in blue) breaks closer to the experimental wave. The overall dynamics of solitary wave run up and breaking are shown satisfactorily, however, the simulation presents some major drawbacks. As well as underestimating the wave height, the geometry of the jet, shown in graph 2, has a rounder jet tip. A reason for this discontinuity could be that the simulation overestimated the effects of the water's viscosity, resulting in a rounded jet. Another reason could be the mesh size at breaking, which might not be fine enough to represent the thin sharp jet of the experimental wave. The smaller wave height can be accounted for in the wave creation process at the inlet. ANSYS (2012) does not provide details on how the 'open channel wave boundary conditions' are imposed. Logically, a



Graph 1. Quantitative comparison of simulated breaking wave with experimental result



Graph 2. Quantitative comparison of simulated vortex creation against experimental result

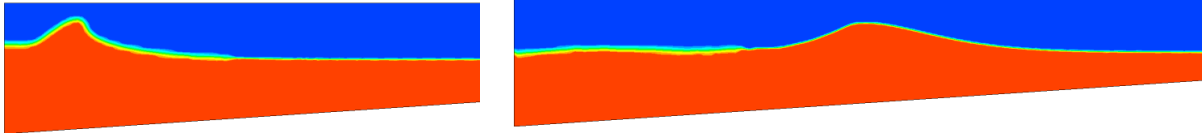


Figure 13. Instability at wave inlet and stability of wave after wave inlet

velocity profile, following Fenton's (1998) equation for solitary waves, should be imposed at the inlet. However, when observing the first instances of the simulation, the wave created was often irregular, propagating vertically as a jet, as shown in figure 13. Only after the wave passed the coarser zone 1 did it stabilize and start propagating with a familiar shape, as a wave approaching the surf zone. The instability caused at the inlet was the primary cause of wave height loss. It also slowed down significantly the wave, causing it to arrive at breakpoint 0.474-0.504 s later than the experiment. By measuring the wave heights at breaking of the simulated triple mesh wave and the experiment, a discrepancy of 15.2% was found. To replicate the experiment, the wave height was raised to $H_0 = 0.1584$ m.

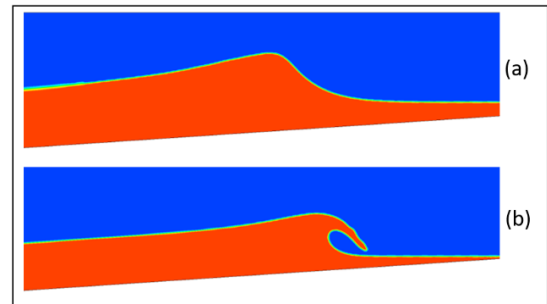
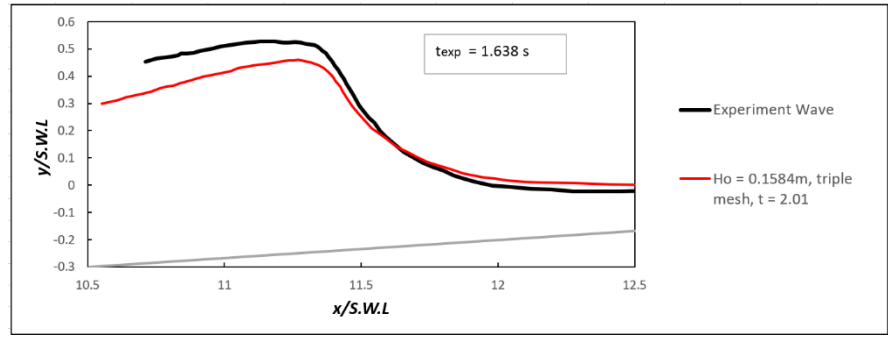


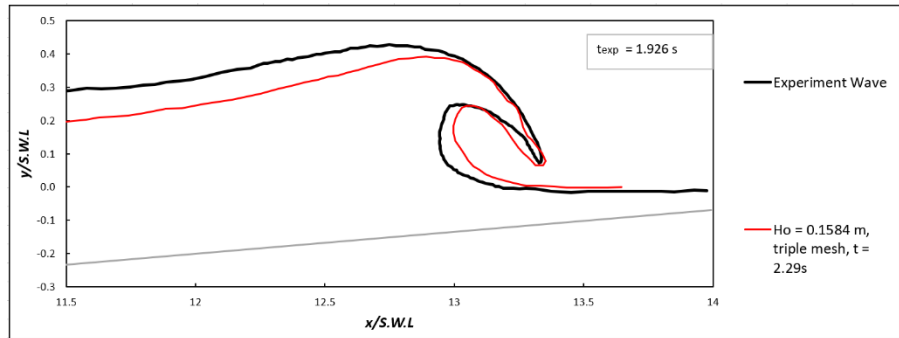
Figure 14. Qualitative snapshot of breaking wave and vortex creation with triple zone mesh and bigger wave.

Figure 14 shows the breaking and vortex creation of the $H_0 = 0.1584$ m wave. By graphing it against the experimental wave it is clear that this simulation was a better representation of Liu's (2000) wave. The main discrepancies lie in a small wave height difference, shown in graph 3, and a slight difference in the geometry of the plunging jet, shown in graph 4.

Although the model underestimated wave height, the wave breaking process occurred at the same x-coordinate as the experiment, showing that the interactions between the bottom slope and the wave particles acted in the same place, forming a slightly smaller wave. The plunging vortex created was very similar



Graph 3. Quantitative comparison of final simulated breaking wave with experimental result.



Graph 4. Quantitative comparison of final simulated vortex creation with experimental result.

to that of the experimental wave. The air entrainment inside the vortex was smaller in the simulated wave and the jet tip of the simulated wave was, once again, more rounded than Liu's (2000) wave. A further discrepancy was shown in the trough of the wave, with the simulated wave showing a lower trough at the back of the wave than the experimental one. This error can be accounted for the nature of the experimental wave. While water particles in ocean waves travel in ellipses and don't move with the wave; the experimental solitary wave was provoked by a displacement, similar to a tsunami, that caused the whole body of water to move, resulting in a wave with no trough. The slight underestimation of the model's wave height was the result of the wave instability at the inlet, which, as shown later, stopped the wave from breaking any higher than $H_b = 0.145$ m. A further error was present in the time at which the simulation reached the breakpoint. The experimental wave broke at $t = 1.638$ s, 0.372 s before the simulation. This time difference was the result of the instability at the inlet, however, the simulation performed the wave breaking process at the same speed of the experiment. If the instance of wave breaking in graph 3 was taken as $t = 0$, the overturning of the jet up to when it first touches the water of the experimental and simulated wave differs by only 0.08 s.

Overall, considering that two waves never break in the same manner, and that, if Liu (2000) was to repeat his experiment, it would not achieve the same exact plunging breaker due to the high non-linearity and complexity of the process, the mathematical model described adequately the dynamics and geometry of wave run-up, breaking and overturning. Even though the model produced a smaller wave than shown in the experiment, the wave breaking process independent of deep water wave height looks accurate.

4.1.2.2. Splash up Process

To observe the splash-up process, 5 snapshots of a 0.122m solitary wave from Liu (2000) have been compared with an analogous simulation. As shown in figure 15, the simulation represents accurately the splash-up process present in the experimental wave. The vortex of the wave impinges the surface in fig 15 (a), where

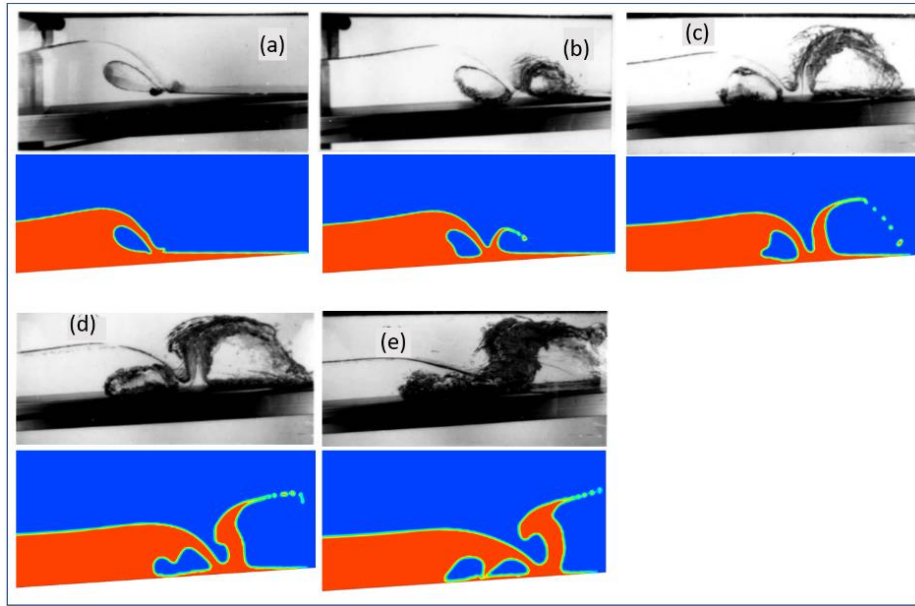


Figure 15. (a) jet first touches water, $t = 2.55$ s. (b) first splash up jet formed, $t = 2.6$ s (c) second air bubble formed, $t = 2.66$ s. (d) wave start collapsing, $t = 2.7$. (e) wave collapses, $t = 2.72$ s

the first clockwise air bubble is created. The wave lip is then reflected in the air to form the second arch and clockwise air bubble in figures 15 (b) and (c). The wave then collapses in itself and the first original air bubble is destroyed with great energy dissipation (Liu, 2000; Keshavarzi et al, 2012) in figures 15 (d-e). Qualitatively, the splash-up process was represented very accurately. The greatest difficulty for the model was to correctly capture the foamy air-water mixture present in the turbulent reflected jet. Here the jet is composed of water particles permeated with very small air bubbles caused from the impact of the first jet in fig. 15 (a). Showing this mixture correctly on Fluent requires an incredibly fine mesh, as singular cells are faced with multiple air and water bubbles, which can't be represented due to the nature of the VOF method.

The present simulation represented, to an adequate precision and within the limits of the geometry, the process of a solitary wave breaking on a 1/15 slope.

4.2. Breaker Intensity Analysis Set up

To investigate the breaking characteristics of solitary plunging waves, 15 waves ranging from 0.04-0.18 m in height have been simulated. The simulations were performed in the same geometry as the validation and the same boundary conditions were imposed. Only the deep water wave height, H_0 , was modified for each case. Table 4 shows the specifications of the different cases, the time period was output by ANSYS based on the effective frequency of the waves, whilst ξ and L_0 were calculated using eqns. 1 and 15, respectively. The time step was set to 0.00025s for 15000 timesteps and a total of 3.75s of simulation.

Table 4. Properties of simulated waves

H_0	Time- Period	L_0	ξ
(m)	(s)	(m)	
0.04	3.584	20.057	1.493
0.05	3.217	16.158	1.198
0.06	2.947	13.556	1.002
0.07	2.737	11.694	0.862
0.08	2.568	10.295	0.756
0.09	2.428	9.203	0.674
0.1	2.309	8.324	0.608
0.11	2.206	7.600	0.554
0.12	2.116	6.990	0.509
0.13	2.035	6.466	0.470
0.14	1.962	6.009	0.437
0.15	1.894	5.602	0.407
0.16	1.831	5.235	0.381
0.17	1.771	4.898	0.358
0.18	1.714	4.585	0.336

5. Results and Analysis

To measure and compare the breaking characteristics of the simulated waves, graphs of different wave characteristics such as the breaker index and the SSP are plotted and compared to expected values. Correlations between different breaking intensity measures are shown and their validity is addressed. Finally, the jet thickness ratio (eqn. 17) is calculated and graphed against the wave characteristics in order to find a correlation to validate this new parameter.

5.1. Qualitative Observations

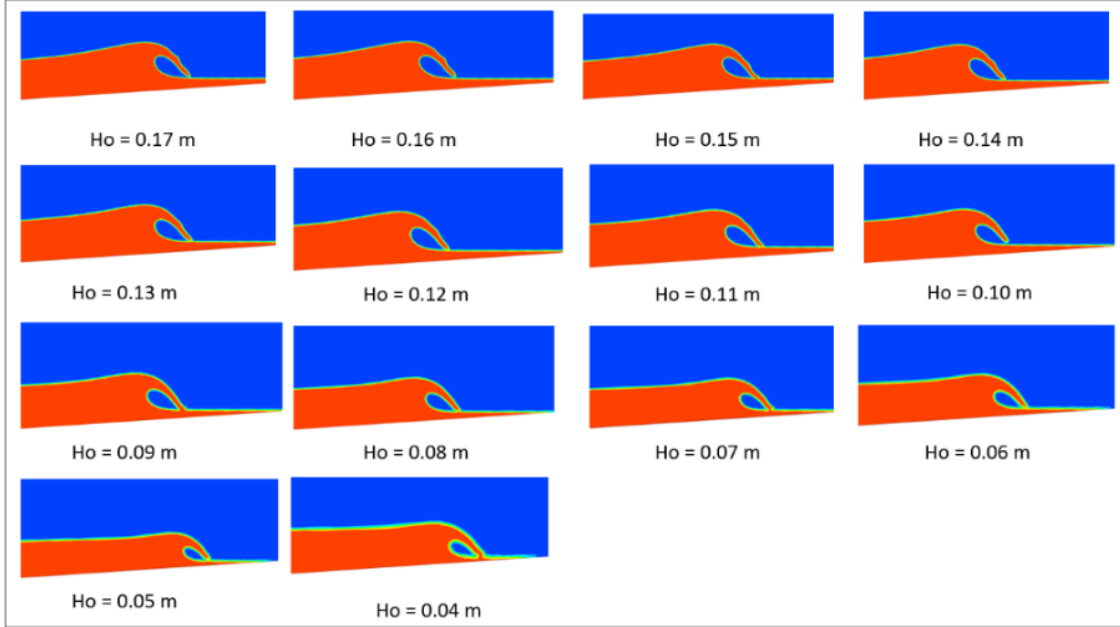


Figure 16. Qualitative comparison of vortex creation of the 15 different cases simulated.

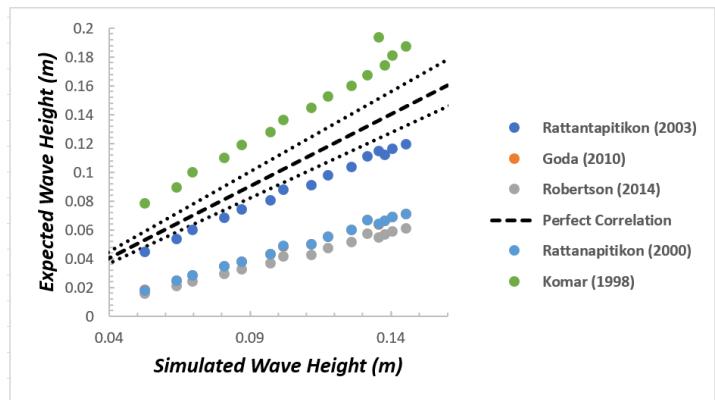
Shown in figure 16 are the snapshots of the simulated waves when the overturning jet first impacts the water. As wave height increased, the mesh resolution increased due to the ratio of cell size to wave height decreasing, causing the coarser details of the bigger breakers to be sharper. Also, as wave height increased the jet of the wave seemed to have small deformations on the outer part that slowly disappeared as the wave approached $H_o = 0.10$ m. This discontinuity in the geometry of the jet could be caused by a variety of reasons. Firstly, surface tension has a greater impact on smaller waves, causing the jet to be less prone to deformation. The lump created on the breaking lip of the waves could be due to refraction and reflection of water at the pressure outlet, causing a reversed flow that could have imposed itself on the breaking wave deforming the lip. As smaller waves are less sharp, this deformation becomes less evident, up to a point where it completely disappears due to the mesh not being fine enough. It can be observed that as the waves became smaller and breaking intensity increased, the plunging vortex created decreased in size. Another interesting finding was that, as deep water wave height was increased over $H_o = 0.11$ m, the resulting breaker height, H_b , was smaller than its deep-water counterpart. The highest breaking wave height recorded was of $H_b = 0.145$ m with deep water wave height $H_o = 0.17$ m. Imposing a higher deep-water wave height resulted in the wave touching the top of the domain at the inlet, losing energy and creating a smaller wave. The underestimation of the larger waves can be attributed to the instability at the inlet causing them to interact with the boundary of the domain.

5.2. Breaker Height and Depth

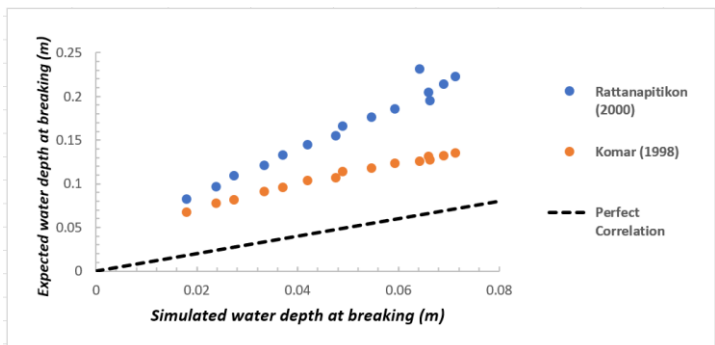
Graphs 5 and 6 show the expected wave height and breaking depth against the simulated results. Wave height and depth at breaking have been measured according to 3.2 and theoretical values have been plotted using eqns. 4-10. As shown in graph 5, the expected wave heights often overestimate the wave height at breaking, especially using Robertson (2014), Rattanapitikon (2000) and Goda (2010). These authors described the wave height as a power law with respect to slope of the breaker and wavelength. However, it seems that the effect of wavelength in these equations overestimated the breaker height. This is due to the small dependency of plunging breakers on wavelength, as their shape is mostly defined by the slope of the seabed (Black and Mead, 2001). Better results were obtained using Rattanapitikon (2003) which lies close to the 10% error and Komar (1998) that underestimates the height of the breakers, contrarily to other authors. The discrepancy lies in the complexity of the wave breaking process, and the effect of reef slope, which changes drastically as the slope increases and plunging breakers start to collapse. However, Rattanapitikon (2003) proposed a fairly correct estimate of the wave height at breaking.

This was not the case with water depth at breaking, shown in graph 6, where a large overestimation of the breaker depth is present. This divergence shows the inefficacy of the current breaker depth equations to quantify the wave breaking process. The error can be associated with the different test conditions and slopes used in Komar (1998) and Rattanapitikon's (2000) work, which often used flatter slopes to observe breakers, which resulted in much higher breaker depths.

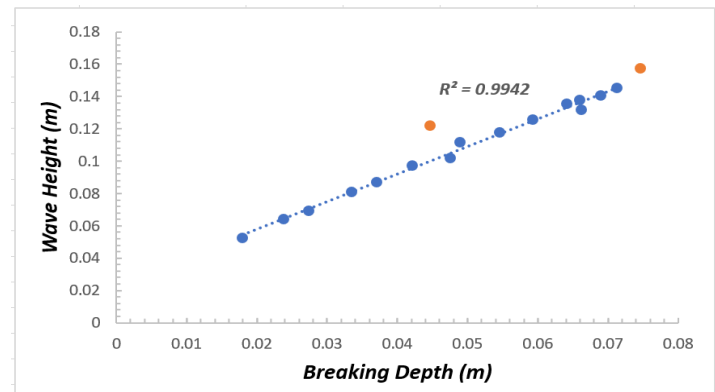
Graph 7 shows the effect of wave height on breaking depth. As expected, the breaking depth increased linearly as the wave height increased, with an R^2 value of 0.9942. The effect of breaker index (eqn. 14) is shown in



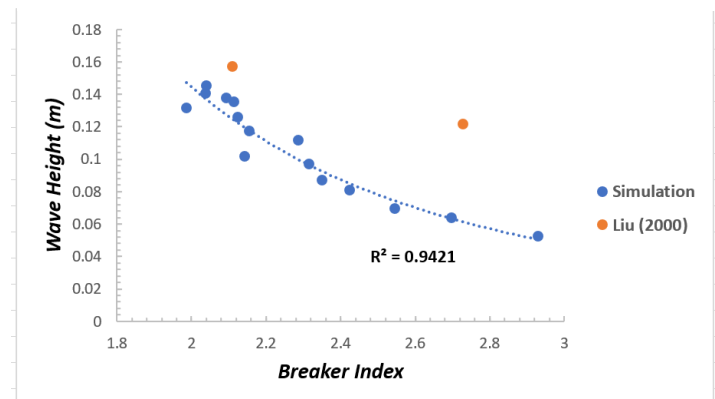
Graph 5. A graph of expected wave height against simulated wave height



Graph 6. Simulated water depth against expected values

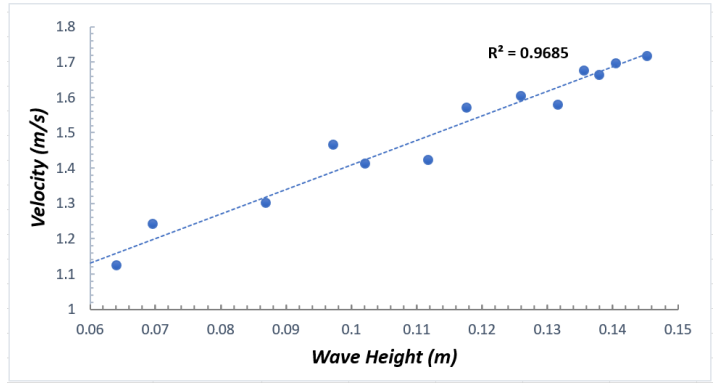


Graph 7. Breaker height against breaker depth of simulations



Graph 8. Breaker height against breaker index of simulated waves

graph 8. As anticipated, the breaker index increased as the wave height decreased, since on the same slope, a smaller wave offers a more intense ride. This relationship is accounted for in the Iribarren number, where a smaller wave height increases its value and, therefore, breaking intensity. The data set follows a power law trend, it can be observed that as the wave height decreased below 0.1 m the breaker index increased at a faster rate. The data agreed well with Liu's (2000) $H_0 = 0.137$ m wave, however, Liu's (2000) $H_0 = 0.091$ m wave exhibits a higher breaker index than its simulated counterparts. This can be due to the displacement wave which manages to retain its shape without breaking up to a higher point on the slope. Liu's (2000) values for breaker index are unprecedented in literature, where plunging breakers only ever break with breaker indices ranging from 1-1.8 (Battjes, 1974; Kaminsky, 1993; Robertson, 2014). This shows the discrepancy between experimental results and the uncertainty present in predicting the intensity of breaking waves.



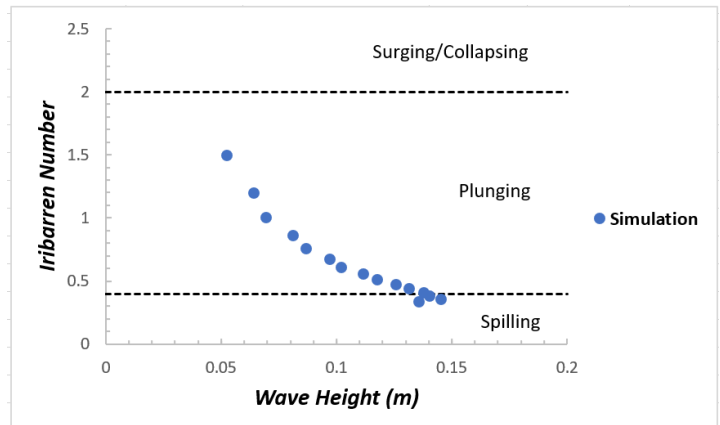
Graph 9. Velocity of wave crest at breaking against breaker height of simulations.

Graph 9 shows the velocity at the wave crest of the simulated waves. Similarly to water depth, velocity increased linearly as wave height increased. The velocity has been recorded just before the jet of the wave detaches from the main body and starts to overturn, therefore, the results show the instance where the water particles reached the celerity of the wave causing it to topple over and break.

5.3. Breaking Intensity

5.3.1. Iribarren Number (SSP)

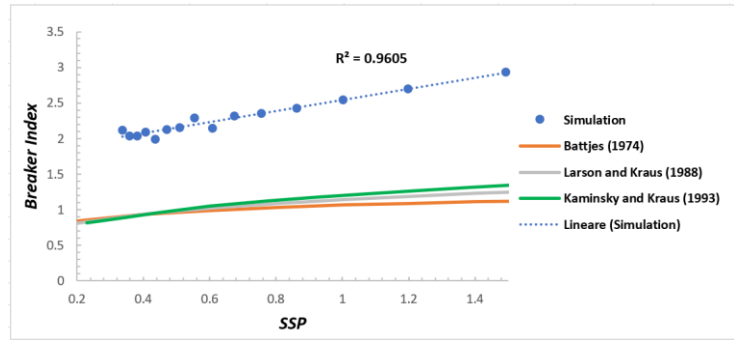
Graph 10 shows the relationship between the Iribarren number and the wave height of the simulated cases. The Iribarren number has been calculated using eqn. 1. As can be observed, most of the simulations fell within the plunging area, correctly describing the shape of the simulated waves. However, in accordance with the literature (Black and Mead, 2001; Robertson, 2014; Johnson, 2009), the bigger waves fell within the plunging-spilling border. This shows the inefficacy of the Iribarren number to distinct plunging breakers from spilling, as all the waves simulated were clearly plunging. The error rises from the dependency of the Iribarren number on the wave length, which, as stated before, has little to no effects on plunging breakers. Contrarily, spilling breakers are highly subject to the wavelength, and are highly dependent on the preconditioning of the wave by the reef slope and orientation in deeper water (Black and Mead, 2000).



Graph 10. Iribarren number of simulated waves against breaker height.

Graph 11 shows the relationship between the breaker index and the surf similarity parameter, calculated using eqn. 2, of the simulated waves. As observed, the breaker index increased linearly with the SSP, showing how

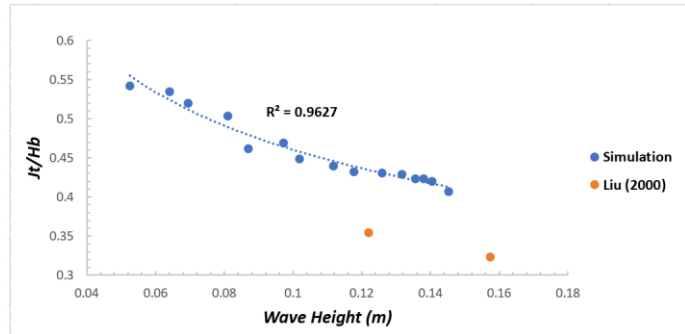
the waves progressed towards the surging/collapsing border as they broke in shallower water. Literature values from different authors are plotted on graph 11. The curve shapes are similar to the simulated cases; however, the breaker indices show much smaller values. This discrepancy could be due to the flatter slopes used by the authors, which resulted in wave breaking in deeper waters. Liu's (2000) experimental value could not be plotted due to the unavailability of wavelength to calculate the SSP, however, it can be noted that the breaker indices produced by Liu's waves were much higher than those found in literature. Therefore, it can be concluded that the breaker indices calculated from the simulations, even though in strong disagreement with literature values, do exist in nature given certain conditions. The current breaker intensity parameters fail to fully describe the breaking characteristics of plunging breakers, often creating diverse breaking conditions for what was categorized as the same breaker, showing the need for quantitative methods to better characterise breaking waves.



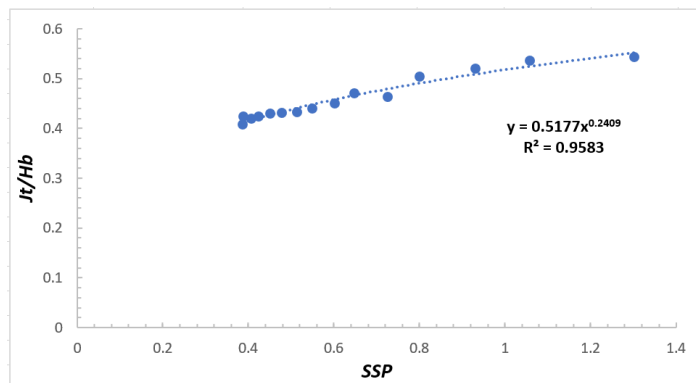
Graph 11. Breaker index against SSP of simulated waves

5.3.2. Jet Thickness Ratio

Graph 12 shows the effect of wave height on the jet thickness ratio. The jet thickness ratio has been calculated as described in 3.2. As observed, the jet thickness ratio decreased as the wave height increased following a power law trend with an R^2 value of 0.9627. This result agreed with the expected theory, showing that as breaking intensity increased in smaller waves, the jet thickness ratio also increased. This is further demonstrated by graph 13, that shows an increase in jet thickness ratio as the SSP increases. The results show a clear trend between the breaker intensity of a wave and its jet thickness ratio, showing that this novel parameter could be used to reinforce and reestablish the knowledge of breaking intensity of plunging breakers. However, it must be noted that there were various errors present in the simulation that could have tampered with the results obtained. As shown in the validation, the geometry of the plunging jet does not replicate the experiment precisely, jeopardizing the validity of the geometrical parameter. This is shown in graph 12, where the jet thickness ratios of Liu's (2000) experimental waves are plotted. Clearly, the simulation overestimated the thickness of the jet produced; however, the relationship between wave height and jet thickness ratio is maintained. The validity of this method is assessed in the discussion



Graph 12. Jet thickness ratio against breaker height of simulations.



Graph 13. Jet thickness ratio against SSP of simulations

6. Discussion and conclusions

6.1. Discussion

6.1.1. Suitability of ANSYS

Overall, ANSYS Fluent provides good means to simulate the process of solitary waves breaking in the surf zone. The overall dynamics of the wave run up and overturning have been simulated to a good degree of accuracy, and the splash-up process was very well defined. However, limitations to the functionality of ANSYS are present.

Firstly, the mesh dependence of wave formation and breaking renders incredibly difficult the succession of the simulation. As stated earlier, by changing the mesh slightly the wave breaking process was compromised and, in most cases, disappeared completely. Not only does the mesh size control the interface sharpness, crucial to correctly simulate the geometry of the overturning waves, it also controls the speed and stability at wave inlet. Having the wrong mesh at the inlet means that the wave enters the domain unstably, often breaking and causing most of the wave energy to be dissipated, resulting in an incredibly smaller wave than expected. The discrepancy in wave height probably arises from the wrong mesh dimension at inlet, causing some of the wave energy to be lost, and the resulting breaker being smaller than expected.

The main limitation to the completion of the project was the computational expense. Even though it is not contiguous to ANSYS, but rather to the machine used to simulate, the high computational expense encountered in simulating waves limited the findings of this dissertation. The higher order schemes used in discretizing the governing equations, together with the CLSVOF method coupled with the transient formulation are some of the reasons for this high expense. The simulations were performed using a server machine with 28 Xeon core processors, which represented a significant power source. However, each 2D simulation still took over 5 hours, with another 2 hours of download time of the results from the server machine.

The high computational expense incurred coupled with the strict mesh dependence meant that the author was unable to formulate any other geometries with different slopes. The long waiting time made a mesh convergence study unfeasible, and the right mesh had to be found by trial and error. Moreover, simulating in 3D, which was the original scope of the thesis, was impossible with the given computational resources. Not only would such a simulation take over two weeks, but the data created for post-processing would weigh over 1.5 Terabytes.

Finally, the unavailability of using a second order time discretization with the CLSVOF means that coupling this method with a LES turbulence model was unachievable on ANSYS. To achieve the best results, other open source codes such as OpenFoam should be used. However, given the right computational power, ANSYS is a powerful tool to simulate solitary waves and this work could be extended to other geometries and in 3D. To do so, especially in 3D, a supercomputer with hundreds of processors would be needed.

6.1.1. Breaking Wave Characteristics

The breaking characteristics of 15 different waves have been simulated and analysed, with results displaying the right relationships with respect to theory. The breakers generally behaved correctly, increasing in intensity as they got smaller. However, the study has some great limitations arising from the simulation and the existing theory, which results in a high degree of uncertainty and some substantial errors in the analysis.

Above all, the discrepancy in the validation of the code with the model slightly underestimating, by roughly 7%, the height of the wave, means that the measurements done on the wave were not realistic. This resulted in smaller breaker indices than the experimental values, which, given the use of steeper slope and displacement wave, were much higher than normal literature values. Also, although the $H_0 = 0.137$ m wave was validated sufficiently, this does not mean that the other smaller breakers were simulated correctly. As shown in graph 7, Liu's (2000) smaller breaker does not break exactly according to the simulation, even though the geometry used was the same.

Moreover, as pointed out by De Schipper (2012), waves under 10 cm in height start to suffer from scale effects, with surface tension playing an increasingly important role and morphing the dynamics of wave breaking. Also, the discrepancy in definition of wave height at breaking used by authors throughout literature, with some authors defining the breaking point as when the wave crest becomes vertical (Sayce, 1998) and others describing it as when the wave celerity is matched by the water particle velocity (Johnson, 2009; Robertson, 2014), comparing simulation with literature values is dependent with the methodology used. Furthermore, some of the theories used to predict breaker height and depth (Robertson, 2014) have been used outside the conditions they were stipulated in, causing a further source of error.

To overcome the deficiency in the simulated waves, a User Defined Function (UDF) could have been used. The UDF is compiled manually and specifies, through the use of macros commands, the velocity and surface profiles created by imposing Fenton's Solitary wave theories. This could ensure greater stability at the inlet, as the velocity equations have been imposed manually and can be checked for errors.

Overall, the main limitations of the SSP and breaker index have been demonstrated, with the uncertainty of the SSP in the transitional areas confirmed and high values of breaker index in a supposedly 'spilling' area.

6.1.2. Jet Thickness ratio

To better understand the intensity and characteristics of plunging breaking waves, the jet thickness ratio has been proposed. Although very simplistic in nature, this parameter showed some promising results that form the benchmark for describing breakers in term of their geometrical properties. However, due to the following reasons, the author did not quantify this parameter or form relationship with respect to other breaking parameters of the waves.

Firstly, the discrepancy of the geometry of the overturning jet, showed in the validation, means that this parameter is very inaccurate. This is shown in graph 12, where the experimental waves show a much smaller jet thickness ratio than the simulated ones. Moreover, the lack of different slopes used tampered with the understanding of this parameter, which is very dependent on reef slope. For a better understanding of this geometrical parameter, different geometries, wave heights and wavelengths could be simulated to validate its usefulness and practicability, with legitimate relationships drawn.

The simplicity coupled with the small amount of data generated, renders this parameter a first estimate at differentiating between different intensities of plunging breakers. However, it proposes a simple measurable relationship, that, if studied further and more contiguously, can enhance the knowledge of breaking waves.

6.2. Conclusion

Overall, this thesis has managed to explore wave breaking characteristics of different plunging breakers with the use of numerical simulations. ANSYS has been used and evaluated as a tool to simulate the complex process of wave overturning and different wave breaking conditions have been explored and compared to the

existing theory. A novel parameter has been introduced, and comments on its' suitability and simplicity have been made. The following conclusions have been drawn:

- ANSYS fluent is a powerful tool to describe solitary wave run up and overturning and, given the right computational power, can be used to simulate 3D sections with complex topography as well as different 2D geometries. The sole limitation of ANSYS is the incapability of using higher order transient formulation schemes needed for LES when using the VOF model.
- The code implemented simulated satisfactorily breaking conditions on a 1/15 slope, with the general dynamics represented accurately and the breaking characteristics relationships expected achieved.
- The main limitations of the existing breaking intensity theories have been demonstrated, showing that a single, easily implementable parameter to describe wave breaking occurrence is still missing in the present literature.
- The jet thickness ratio, a novel parameter describing the breaker intensity of the wave in terms of the geometrical properties of the plunging breaker has been introduced. Within its limitations, this parameter shows good correlation with existing breaking intensity theories, showing its potential to extend the knowledge of plunging breakers. Deemed as simplistic and lacking the statistical dependence to quantify the validity of this method, this dissertation provides a benchmark for further research to be taken on this topic.

The aims and objectives presented in the introduction have all been addressed, except for the first point, where different bottom topographies have not been simulated, due to the strict meshing dependency and computational expense incurred in the project. Further recommendations include:

- Perform a mesh convergence study to understand the relationship between mesh size and wave formation to enhance stability of waves at the inlet of the geometry.
- Evaluate different turbulence methods for the correct representation of the breaking process.
- Simulate waves breaking over different seabed topographies to show the effect of bottom slope on wave breaking characteristics.
- Continue research in jet thickness ratio, including effects of different bottom slopes, wave heights and wave lengths to produce a statistically sound relationship between jet thickness ratio and the intensity of plunging breakers.
- Simulate 3D topographies to analyse and evaluate different surfing conditions, exploring peel angles, effects of refraction and reflection and surf-ability.

7. Project management, consideration of sustainability and health and safety

7.1. Project Management and Sustainability

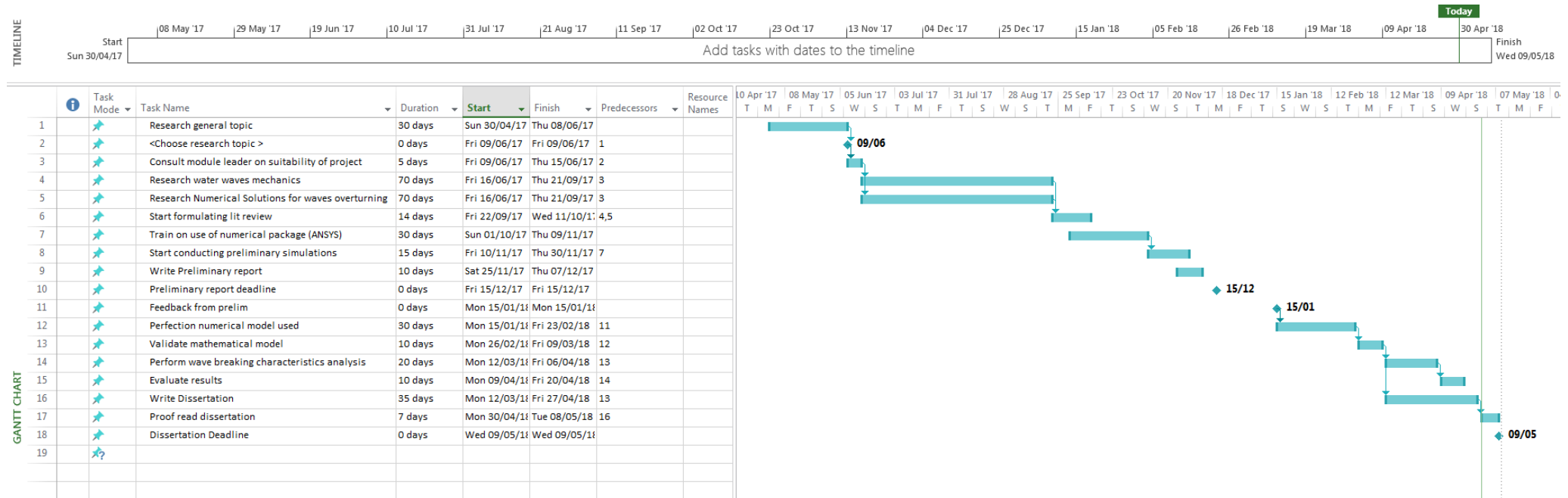


Table 5. Gantt Chart used for project planning and management

Shown above is the Gantt chart followed for the correct completion of the project. It has been modified since the start of the project to suite the changes made throughout the project development. Originally, the scope of this thesis was to simulate 3D sections of waves overturning, evaluating the surfing conditions created and proposing a conceptual wave-pool reef design for optimum surfing performance. Unfortunately, the author failed to simulate in 3D owing to the time restriction and, especially, the high computational expense associated with the complex three-dimensional simulations. This shifted the focus of the thesis to the analysis of plunging breakers in 2D, focusing on quantifying breaking intensity instead of surf-ability of wave sections.

With respect to sustainability, CFD methods were employed to simulate the very complex, hardly measurable natural process of breaking waves. The scarcity of world-class surfing breaks coupled with the complicated and expensive methods to take in-situ measurement of breaking waves makes CFD the best candidate to study this complex phenomenon. Another method to measure breaking wave characteristics would be to perform laboratory experiments in a wave tank. Due to the unavailability of a wave tank and the complexity in creating a physical model, CFD methods were chosen as the final solution.

Even though CFD methods have been chosen for the simplicity in implementation and efficiency, the complexity of the problem resulted in very long simulation times. Maximising time-efficiency without tampering with the strict meshing practice was a great challenge. Solitary wave theories were preferred to the more computational expensive Cnoidal theories, and the coarse mesh zone at the inlet helped increase the efficiency. The completion of this project would have been impossible if simulated on standard desktop computers available in the University, with each 3 second simulation taking over three days to complete. The use of HPC server machines was vital to the achievement of the project aims. However, simulating in 3D would require an even greater computational resource, as the cell count increases from hundreds of thousands to tens of millions, capsizing the potential of the HPC Xeon machines running on all 28 processors available.

7.2. Risk Assessment

A brief risk assessment of the potential and incurred risks associated to the project are shown below. Generally, CFD simulations are virtually risk-free, with small hazards associated to them such as eye strain or back pain from sitting at a monitor too long. However, to mitigate these small risks, the following risk assessment has been performed.

Consequence Score						Risk Score
	1	2	3	4	5	Consequence Score
Descriptor	Insignificant	Minor	Moderate	Major	Catastrophic	
Likelihood Score						×
	1	2	3	4	5	Likelihood Score
Descriptor	Rare	Unlikely	Possible	Likely	Almost Certain	
Frequency	Not expected to occur for years	Expected to occur at least annually	Expected to occur at least monthly	Expected to occur at least weekly	Expected to occur at least daily	1-25
Probability	< 1%	1 – 5 %	6 – 20 %	21 – 50 %	> 50 %	

Table 6. Method to calculate likelihood, consequence and risk score for risk assessment

Table 7. Risk assessment table including a description of the risks being mitigated, hazards encountered, existing control measures and further actions required to control risk.

College			CEMPS	Date	20 /04/2018		
Name			Stefano Conti	Job Title	CFD simulations		
DESCRIPTION			Various months of CFD simulations undergone using the HPC server machines available in CEMPS. All simulations were undergone in the Harrison Building at Exeter University. The main task activities assessed for risk are: the physical time passed in front of a computer simulating or managing hardware, the vast amount of data handling between different platforms and the correct usage of the simulating software				
Ref	Hazard Identification		Existing Control Measures in Place	Consequence	Likelihood	Risk Assessment Score	Further Actions Required to Control Risk
	Hazard	Who and How					
A	Eye Strain from computer display	Author- Eye strain caused by extensive exposure to display lights.	-Avoid continuous exposure – take brakes -Lower luminosity on computer screen	3	2	6	None
B	Fire in Harrison Building	Students and Staff - Fire hazards present in engineering building.	-Make note of fire exits. -Perform fire drills -Be familiar with University fire evacuation policy	5	1	5	None
C	Lone Working	Author - Risk of falling ill or injured with no one around.	-Do not work alone in Harrison - Do not work alone home	4	1	4	None
D	Loss of data	Author - Loss of data through corruption of hard drive or faulty software.	-Ensure hard drive is ejected safely from computer. -Save data on more platforms. -Ensure good connection when transferring data	4	3	12	None
E	Incorrect Usage of CFD software	Loss of progress or data due to malfunction of software due to malpractice	-Do not override ANSYS with tasks -Always ensure good connection when meshing for long periods -Save work often	3	4	12	None

References

1. **Afs.enea.it.** (2018). ANSYS FLUENT 12.0 Theory Guide. [online] Available at: http://www.afs.enea.it/project/neptunius/docs/fluent/html/th/main_pre.htm [Accessed 28 Apr. 2018].
2. **Afs.enea.it.** (2018). ANSYS FLUENT 12.0 User's Guide. [online] Available at: http://www.afs.enea.it/project/neptunius/docs/fluent/html/ug/main_pre.htm [Accessed 28 Apr. 2018].
3. **Battjes, J.** (1974). Surf similarity, *Proceedings of the International Conference on Coastal Engineering*, ASCE, pp. 466 – 480.
4. **K. P. Black and S. T. Mead.** (2001). Classification of Surf Breaks in relation to Surfing Skill. *Special Issue of the Journal of Coastal Research on Surfing*. P66-81
5. **Bowen, A.J., Inman, D.L. and Simmons, V.P.** (1968). Wave "set-down" and set-up. *J. Geoph. Res.*, 73, 8, , p. 2569-2577.
6. **Chen G, Kharif C, Zaleski S, Li J.** (1999). Two-dimensional Navier–Stokes simulation of breaking waves. *Phys. Fluids* 11, 121–133.
7. **Goda, Y.** (2010). Reanalysis of regular and random breaking wave statistics. *Coastal Engineering Journal*, 52(1): 71 - 106
8. **Grilli, S.T., Svendsen, I.A. and Subramanya, R.** (1997). Breaking criterion and characteristics for solitary waves on slopes. *Journal of Waterway, Port, Coastal and Ocean Engineering*, 123(3): 102 -112.
9. **De Schipper, M.** (2007). On the generation of surfable ship waves in a circular pool: Part I. M.Sc. Delft University of Technology.
10. **Fenton, J.** (1979). A high-order cnoidal wave theory. *Journal of Fluid Mechanics*, 94(01), p.129.
11. **Fenton, J.D.** 1998. The Cnoidal Theory of Water Waves. Chapter 2 of *Developments in Offshore Engineering*, Ed. J.B. Herbich, Gulf: Houston, 1998, 2-34
12. **Hendrickson KL.** (2005). Navier-Stokes simulation of steep breaking water waves with a coupled air-water interface. PhD thesis, Massachusetts Institute of Technology, Cambridge, MA, USA.
13. **Hieu PD, Katsutohi T, Ca VT.** (2004). Numerical simulation of breaking waves using a two- phase flow model. *Appl. Math. Model.* 28, 983–1005
14. **Hutt, J. A.** (1997). Bathymetry and Wave Parameters Defining the Surfing Quality of Five Adjacent Reefs. Unpublished Thesis, University of Waikato, New Zealand.
15. **Iribarren, C.R. and Nogales, C.** (1941). Protection des Ports, Section II, Comm. 4, XVIIth Int. Nav. Congress, Lisbon, , p. 31-80. – surf similarity parameter
16. **Iwagaki, Y.** (1968). Hyperbolic Waves and their Shoaling. *Coastal Engineering in Japan*, 11(1), pp.1-12.
17. **Johnson, C.** (2009). THE EFFECT OF ARTIFICIAL REEF CONFIGURATION ON WAVE BREAKING INTENSITY RELATING TO RECREATIONAL SURFING CONDITIONS. Master Of Science. University of Stellenbosch.
18. **Kelly Slater Wave Company.** (2018). Kelly Slater Wave Company. [online] Available at: <http://www.kswaveco.com/> [Accessed 2 May 2018].
19. **Kinsman, B.** (2002). Wind waves. 2nd ed. Mineola, N.Y.: Dover Pub.
20. **Komar, P. D.** (ed.). [1998] *Beach Processes and Sedimentation* (Prentice-Hall).
21. **Kusterle, T.** (2007). Surf Zone Hydrodynamics. [ebook] Ljubljana: University of Ljubljana Faculty of mathematics and physics Department of physics, pp.1-19. Available at: <http://www-fl.ijs.si/~rudi/sola/SZH.pdf> [Accessed 28 Apr. 2018].
22. **Lakehal D, Liovic P.** (2011). Turbulence structure and interaction with steep breaking waves. *J. Fluid Mech.* 674, 522–577^[17]_{SEP}
23. **Lim, H., Chang, K., Huang, Z. and Na, B.** (2015). Experimental study on plunging breaking waves in deep water. *Journal of Geophysical Research: Oceans*, 120(3), pp.2007-2049.
24. **Liu, Y. and Yu, X.** (2016). A coupled phase-field and volume-of-fluid method for accurate representation of limiting water wave deformation. *Journal of Computational Physics*, 321, pp.459.
25. **Lubin, P., Vincent, S., Abadie, S. and Caltagirone, J.** (2006). Three-dimensional Large Eddy Simulation of air entrainment under plunging breaking waves. *Coastal Engineering*, 53(8), pp.631-655.
26. **McGowan, J.** (1891). On the solitary wave. London, Dublin and Edinburgh, *Philosophical Magazine*, Ser 5, Vol. 32, p.45.
27. **Mead, S. T. & K. P. Black.** (2000)a. Field Studies Leading to the Bathymetric Classification of World-Class Surfing Breaks. *Special Issue of the Journal of Coastal Research on Surfing* p5-20.
28. **Mead, S.** (2003). Keynote address: Surfing Science, *Proceedings of the 3rd International Surfing Reef Symposium*, Raglan, New Zealand, June 22-25, 2003. p1-36
29. **Miche, A.** (1944). Mouvements ondulatoires de la mer en profondeur constant ou décroissante. *Annales des ponts et chaussées*. pp. 25-78, 131-164, 270-292, 369-406
30. **Mortensen, S. and Henriquez, M.** (2012). Advanced Numerical Modelling of Artificial Surfing Reefs. *The reef Journal*, 2(1176-7812), pp.64-84
31. **Mutsuda H, Yasuda T.** (2000). Numerical simulation of turbulent air-water mixing layer within surf-zone. In *Proc. 27th Int. Conf. on Coastal Engineering*, vol. 1, pp. 755–768. Sydney, Australia: ASCE.
32. **Olsson, E., Kreiss, G. and Zahedi, S.** (2007). A conservative level set method for two phase flow II. *Journal of Computational Physics*, 225(1), pp.785-807.
33. **Peng, D., Merriman, B., Osher, S., Zhao, H. and Kang, M.** (1999). A PDE-Based Fast Local Level Set Method. *Journal of Computational Physics*, 155(2), pp.410-438.
34. **Rattanapitikon, W. and Shibayama, T.** (2000). Verification and modification of breaker height formulas. *Coastal Engineering Journal*, 42(4): 389 – 406
35. **Rattanapitikon, W. and Shibayama, T.** (2003). Breaking wave formulas for breaking depth and orbital to phase velocity ratio, *Coastal Engineering Journal* 48(4), 395–416.
36. **Robertson, B., Hall, K., Zytner, R. and Nistor, I.** (2013). Breaking Waves: Review of Characteristic Relationships. *Coastal Engineering Journal*, 55(1), pp.1350002-1-1350002-40.
37. **Robertson, B., Nistor, I., Hall, K. and Buckham, B.** (2014). REMOTE MEASUREMENT AND PREDICTION OF BREAKING WAVE PARAMETERS. *Coastal Engineering Proceedings*, 1(34), p.41.
38. **Sayce, A., Black, K. & Gorman, R.** (1999) "Wave breaking shape on surfing reefs," *Coasts and Ports Conference 1999*, Perth, Australia, pp. 596–603
39. **The Tokyo Organising Committee of the Olympic and Paralympic Games.** (2018). Olympic Sports : Surfing | The Tokyo Organising Committee of the Olympic and Paralympic Games. [online] Available at: <https://tokyo2020.org/en/games/sport/olympic/surfing/> [Accessed 28 Apr. 2018].
40. **Walker, J. R.** (1974a). Recreational Surf Parameters. LOOK Laboratory TR-30, University of Hawaii, Department of Ocean Engineering, Honolulu, Hawaii, 1974.
41. **Walker, J. R.** (1974)b. Wave Transformations Over a Sloping Bottom and Over a Three-Dimensional Shoal. PhD. Dissertation, University of Hawaii, 1974
42. **Wang Z, Zou Q, Reeve DE.** (2009). Simulation of spilling breaking waves using a two phase flow CFD model. *Comput. Fluids* 38, 1995–2005.
43. **Wang, Z., Yang, J., Koo, B. and Stern, F.** (2009). A coupled level set and volume-of-fluid method for sharp interface simulation of plunging breaking waves. *International Journal of Multiphase Flow*, 35(3), pp.227-246
44. **Wavegarden.com.** (2018). Wavegarden. [online] Available at: <http://wavegarden.com/> [Accessed 2 May 2018].
45. **Xie, Z.** (2015). A two-phase flow model for three-dimensional breaking waves over complex topography. *Proceedings of the Royal Society A: Mathematical, Physical and Engineering Science*, 471(2180).

